https://doi.org/10.5194/egusphere-2026-2034
Preprint. Discussion started: 27 May 2026

Milankovitch Forcing and Nonlinear Climate Variability during the Late Givetian (Appalachian Basin, New York, USA)

Jarno J.C. Huygh[1], Carlton E. Brett[2], James J. Zambito IV[3], Ian J. Forsythe[2], Loïc Sablon[4], Justin Gérard[4], Michel Crucifix[4] and Anne-Christine Da Silva[1]

[1] SediCClim Laboratory, Department of Geology, Liège University, Liège, Belgium

[2] Department of Geosciences, University of Cincinnati, Ohio, United States of America

[3] Department of Geology, Beloit College, Wisconsin, United States of America

[4] Earth and Life Institute, UCLouvain, Louvain-la-Neuve, Belgium

Correspondance to: Jarno Huygh (jarno.huygh@uliege.be)

Key Points:

- High- and low-latitude climatic and hydrological teleconnections shaped Late Givetian climate variability
- Linear and nonlinear (half)precession-obliquity interactions governed climate-sediment responses in the pantropical belt
- Astronomical forcing paced regional events and the timing of the Frasnes Crisis in the Appalachian Basin

https://doi.org/10.5194/egusphere-2026-2034
Preprint. Discussion started: 27 May 2026

Abstract

Astronomical forcing is a major driver of Earth's climate variability, yet the linear and nonlinear climate responses to this forcing under warmer-than-present conditions remain poorly constrained. We use cyclostratigraphy of the Sherburne Formation, a Givetian record from the Appalachian Basin, to characterize Milankovitch cyclicity and evaluate the complex climatic behavior inferred from the sedimentary record. A new cyclostratigraphic age model refines the timing of the regional Fir Tree, Hubbard Quarry and Lodi events and places the onset of the global Frasnes Crisis (represented by the regional Lodi Event) into an astronomically calibrated framework. Our results reveal precession-eccentricity-paced detrital influx, obliquity amplification, precession-obliquity interference patterns, half-precessional cyclicity, and nonlinear climate-sediment dynamics. These findings show how pantropical late Givetian climate variability is shaped by high- and low-latitude climatic and hydrologic teleconnections and highlight the sensitivity of Devonian climate to orbital variability.

Keywords: Cyclostratigraphy, Devonian, Orbital Forcing, Nonlinear, Half Precession

https://doi.org/10.5194/egusphere-2026-2034
Preprint. Discussion started: 27 May 2026

Plain Language Summary

Earth's climate is influenced by predictable changes in its orbit around the Sun and variations in its rotational axis. These are known as Milankovitch cycles (precession, obliquity and eccentricity) and shape climate patterns over tens of thousands to millions of years. We studied rocks from the Sherburne Formation in the Appalachian Basin (New York State, USA) to see how these orbital cycles affected climate during the late Givetian, about 380 million years ago, when Earth's climate was in a warmer-than-present state. We show that the late Givetian climate responded strongly to changes in the Earth's orbit. The rocks recorded clear signals of precession, obliquity, and eccentricity, including complex interactions and amplified responses that point to nonlinear climate behavior. Using these patterns, we built a new timeline for several important events during the investigated interval. Overall, our results reveal that the late Givetian climate was highly sensitive to orbital variations, and that these astronomical rhythms played a key role in shaping environmental change and biological turnover.

https://doi.org/10.5194/egusphere-2026-2034
Preprint. Discussion started: 27 May 2026

1. Introduction

Earth's climate system is fundamentally shaped by interactions among astronomical forcing, large-scale atmospheric and oceanic circulation, the hydrological cycle, and internal feedbacks (e.g., Saltzman, 2002). Astronomical forcing refers to the modulation of incoming solar radiation (insolation) caused by quasi-periodic variations in Earth's orbital parameters – precession, obliquity, and eccentricity (Milankovitch 1941). These 'predictable' Milankovitch cycles alter both the amount and latitudinal distribution of insolation (Berger, 1987; 1988; Laskar et al., 2004), strongly influencing seasonality and long-term climate patterns, and they form a cornerstone of our understanding of past climate change (e.g., Hays et al., 1976). However, the climatic expression of astronomical forcing is rarely a simple linear response to insolation changes (Rial et al., 2004). Complex Earth-system dynamics can modulate, amplify or reshape orbital signals across a wide range of timescales (e.g., Imbrie and Imbrie, 1980; Paillard, 1998). Such relationships are increasingly well understood in more recent Cenozoic records (e.g., Lourens et al., 2005; Sullivan et al., 2023) but less so in the Paleozoic (De Vleeschouwer et al., 2024). Recent work has documented the influence of orbitally forced climatic cycles on Devonian paleoenvironmental patterns (e.g., De Vleeschouwer et al., 2012; 2014; Da Silva et al., 2020; Wichern et al., 2024; Gérard et al., 2025; 2026; Huygh et al., 2026), but with a focus on major anoxic or extinction intervals (e.g., the Kellwasser Crisis). Typically, cyclostratigraphic studies apply linear time-series analysis and spectral tools, such as bandpass filtering and continuous wavelet transforms (e.g., De Vleeschouwer et al., 2012; Laurin et al., 2015; Arts et al., 2024; Spiering et al., 2024), to detect Milankovitch pacing of sedimentary cyclicity. Such approaches, however, are not designed to resolve the nonlinear feedbacks which may be responsible for the observed variability. Consequently, their influence on the expression of orbital forcing in Paleozoic climate records remains poorly constrained.

In this work, we investigate how astronomical forcing shaped late Givetian paleoclimate using an approach that allows us to detect both linear and potential nonlinear expressions of Milankovitch cyclicity preserved within the Sherburne Formation (lower

https://doi.org/10.5194/egusphere-2026-2034
Preprint. Discussion started: 27 May 2026

Genesee Group) of central New York State (Baird et al., 2023). The Sherburne Formation represents a well-preserved archive of late the Givetian subtropical Appalachian Basin, making it well suited for evaluating the expression of orbital forcing outside major extinction intervals. Within this framework, we employ high-resolution proxies for detrital input, to analyze the character and frequency structure sedimentary cycles observed within the Sherburne Formation and develop two complementary floating astrochronologies. In addition, we put the regional Fir Tree, Hubbard Quarry and Lodi eustatic and hypoxic events into an integrated sequence- and cyclostratigraphic framework and assess phase relationships between astronomical forcing and paleoclimatic response. Together, these analyses illustrate a workflow that may be broadly applicable to Paleozoic climate archives and show how astronomical forcing and internal Earth-system dynamics interacted to shape the late Givetian paleoclimate.

https://doi.org/10.5194/egusphere-2026-2034
Preprint. Discussion started: 27 May 2026

2. Geological Setting

The Cargill Salt Company Test Core #17 (hereafter Cargill #17 Core) was drilled in 1977 near Lansing, Tomkins County, southern Cayuga Lake area in central New York State, USA (42°31'22.9" N, 76°30'17.5" W) and spans ~847 m of strata, providing a detailed sedimentary record through the upper Silurian to Middle Devonian strata of the northern Appalachian Basin. Deposition of the Sherburne Formation (uppermost Givetian) occurred in a foredeep setting of this foreland basin, which developed during early Tectophase 4 of the Acadian Orogeny and lay within an expanded subtropical zone at approximately 30° S paleolatitude (Fig. 1; Ver Straeten, 2010; Baird et al., 2023; Ver Straeten et al., 2023).

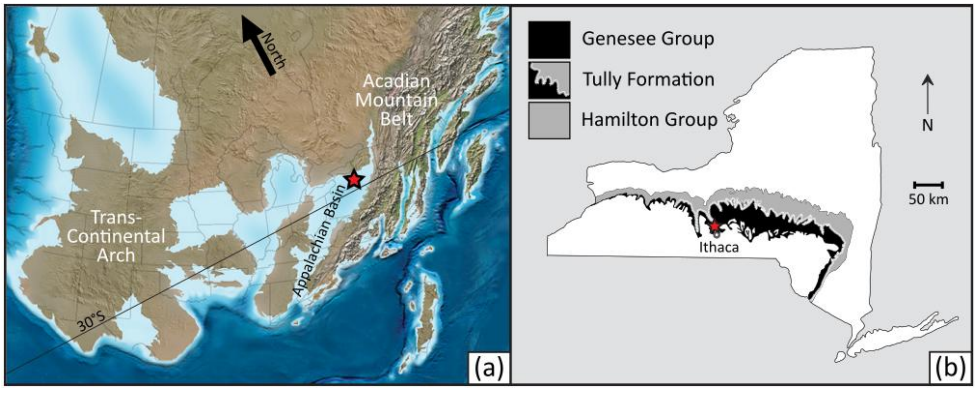

Fig. 1. Geological setting of the Cargill #17 Core. a) Middle Devonian paleogeographic map adapted from Blakey, 2014 (~380 Ma). b) Outcrop belt for the Genesee, Tully and Hamilton in the Appalachian Basin of New York State. Location of the Cargill #17 Core, just north of Ithaca, is indicated by a red star. Figure adapted from Zambito et al. (2016).

The depositional setting of the Sherburne has been interpreted in various ways, traditionally characterized as part of the northern Appalachian Basin Portage Magnafacies that formed on the distal shelf, slope, and proximal basin through turbiditic processes (Rickard, 1975; deWitt and Colton, 1978; see summary in Baird et al., 2023). However, recent work by Wilson and Schieber (2014; 2015; 2017) has interpreted the turbidites of the Sherburne Formation in the Cargill #17 core to more specifically represent fluvial-discharge events deposited in a storm-dominated proximal shale setting through hyperpycnal processes with a

https://doi.org/10.5194/egusphere-2026-2034
Preprint. Discussion started: 27 May 2026

high sedimentation rate. Importantly for this study, hyperpycnites are dependent on flood frequency and magnitude, and therefore climate (Mulder et al., 2003).

The uppermost part of the Cargill #17 Core covers ~41.3 m of the Upper Givetian Sherburne Formation, attributed to the upper portion of the third-order sequence Giv-5 (Brett et al., 2011). Lithostratigraphic correlations and conodont biostratigraphy date the Sherburne Formation from 379.2 to 380.0 Ma (*K. disparilis* to *S. norrisi* zones) (Kirchgasser, 1994; Brett et al., 2011; Becker et al., 2020). Stratigraphically, the Sherburne Formation in the southern Cayuga Lake area comprises the Fir Tree, Hubbard Quarry, and Lodi members, as well as an upper, unnamed Penn Yan Formation-equivalent that is not present in the Cargill #17 Core (Fig. 2; Zambito et al., 2009; Baird et al., 2023). The Sherburne Formation is a time transgressive unit, the base of which generally gets older to the east and south along the outcrop belt in the northern Appalachian Basin and replaces the basinal shale of the Penn Yan Formation through progradation (Baird et al., 2023). The Fir Tree Member (lower *K. disparilis* conodont Zone) in this core consists of medium gray calcareous siltstones to laminated silt and dark shales, marking the onset of subsequence Giv-5D and representing a 3rd order late highstand systems tract (LHST) (previously designated as Giv-5C Brett et al., 2011; but elevated to Giv-5D in Baird et al., 2023). The base of the Fir Tree (subsequence Giv-5D boundary; Fig. 2) is a widely recognized erosion surface marked in cratonic successions by deep incision, for example at the base of the Coralville Formation of the Cedar Valley Group in Iowa (Witzke et al., 1988; Witzke and Bunker, 1996, 1997). The Fir Tree Event therefore represents a regionally recognized event in at least eastern North America, however this event is poorly characterized and not recognized in most recent tabulations of Devonian events (e.g., Becker et al., 2016, 2020; Baird et al., 2023) and may have been conflated with the Geneseo Event of the Taghanic Crisis in studies outside of the Appalachian basin (the Genesee Event is now understood to have been earlier in the *S. hermanni* Zone). However, some workers have noted the beginnings of decline of reefal organisms associated with widespread anoxia toward the end of the *K. disparilis* or *P. dengleri* Zone, with reefal collapse noted at the end of

https://doi.org/10.5194/egusphere-2026-2034
Preprint. Discussion started: 27 May 2026

the Givetian (Copper and Scotese, 2003); it also marks the end of most trilobites in the Appalachian Basin, notably *Dipleura* (Zambito et al., 2015; Baird et al., 2023).

The contact between the Fir Tree and the overlying Hubbard Quarry Member (at 38.3 m depth; Fig. 2) marks a maximum starvation surface (MSS) and minor discontinuity (Brett et al., 2011; Baird et al., 2023); using the sequence stratigraphic model proposed by Zambito et al. (2009) for these strata, the transgression continues through to the base of the middle Hubbard Quarry, which is identified as the maximum flooding surface (MFS) at 28.3 m depth (Fig. 2). While in more distal settings within the Appalachian Basin the deepest, most anoxic conditions of the Hubbard Quarry occur at or near the contact with the Fir Tree, progradation into the study location means the environmental expression of the Hubbard Quarry occurs closer to the MFS (Fig. 2). The Fir Tree – Hubbard Quarry Member succession (*K. disparilis* to *P. dengleri saggita* conodont zones) therefore represents a 3rd order transgressive to highstand to falling stage systems tracts (TST-HST-FSST) (Brett et al., 2011; Baird et al., 2023). It comprises: (i) lower Hubbard Quarry dark gray shales with light gray silty stringers, (ii) a middle subunit composed of alternating dark and lighter gray shales containing crinoids and, (iii) upper Hubbard Quarry gray calcareous siltstones. From 17.7 m upwards, thin traces of cross-lamination are visible, suggesting a higher-energy environment, interpreted as storm-influenced hyperpycnites by Wilson and Schieber (2014; 2015; 2017). After an initial deepening (lower Hubbard Quarry through lowest middle Hubbard Quarry Member), the middle-upper Hubbard Quarry Member displays a significant regressive phase of sediment aggradation (Fig. 2; Baird et al., 2023).

The Lodi Member (10.8 m to 0.8 m depth, *P. dengleri dengleri* to *S. norrisi* conodont zones) consists of medium light gray, slightly bioturbated, calcareous siltstone with abundant *Aulopora* and represents a 3rd order transgressive systems tract (TST) (Brett et al., 2011). The onset of the Frasnes Crisis (Becker et al., 2020) coincides with the base of the Lodi Member and is marked by the regional Lodi Event, which represents another major lowstand sequence boundary. Indeed, a major incised erosion surface of up to 18 meters is observed at the base

https://doi.org/10.5194/egusphere-2026-2034
Preprint. Discussion started: 27 May 2026

Lithograph City Formation (middle Cedar Valley Group) in Iowa (Witzke et al., 1988; Witzke and Bunker, 1996, 1997). The uppermost Lodi Member (*S. norrisi* conodont Zone, uppermost Givetian) is absent in the Cargill #17 Core, so the Givetian-Frasnian boundary is most likely not recorded. The uppermost ~3.8 m of the core are fragmented, with multiple missing intervals.

The Frasnes Crisis was multi-phased with three pulses of extinction, each associated with a transgression and widespread dysoxic-anoxic events. The first phase occurred at the later *P. dengleri* to *S. norrisi* zone, the age of the Lodi Member and just prior to the Givetian-Frasnian boundary. The largest phase is associated with black shales of the early Frasnian MN-1 zone and a final event in the lower MN-2 zone (see e.g., Klapper, 1989 regarding Montagne Noire (MN) conodont zonation). The early phase, which is regionally called the Lodi Event, includes major ammonoid extinction and termination of reef growth in many areas (Becker et al., 2016, 2020).

The Sherburne Formation records environmental characteristics of the late Givetian. This interval is broadly regarded as a warm-temperate greenhouse world (Becker et al., 2020), although recent work by Dahl et al. (2022) challenges this view: CO_2 reconstructions and climate-sensitivity modeling suggests that the Givetian climate may have been cooler and more variable than previously thought. The Givetian was marked by the expansion of tree-like terrestrial vegetation (e.g., *Archaeopteris*; Stein et al., 2020), and considerable faunal turnover that shaped evolutionary steps in the marine realm (Raup and Sepkoski, 1982; House 2002; Brett et al., 2020; Becker et al., 2020; Ver Straeten et al., 2023). Regionally, the Sherburne Formation captures environmental variability following the major, second-order Taghanic Crisis and leading into the onset of the second-order Frasnes Crisis (Brett et al., 2011; 2020; Zambito et al., 2012, 2016; Becker et al., 2016, 2020; Baird et al., 2023). These broader climatic and biotic conditions provide the environmental backdrop against which the Sherburne Formation's cyclicity is evaluated.

https://doi.org/10.5194/egusphere-2026-2034
Preprint. Discussion started: 27 May 2026

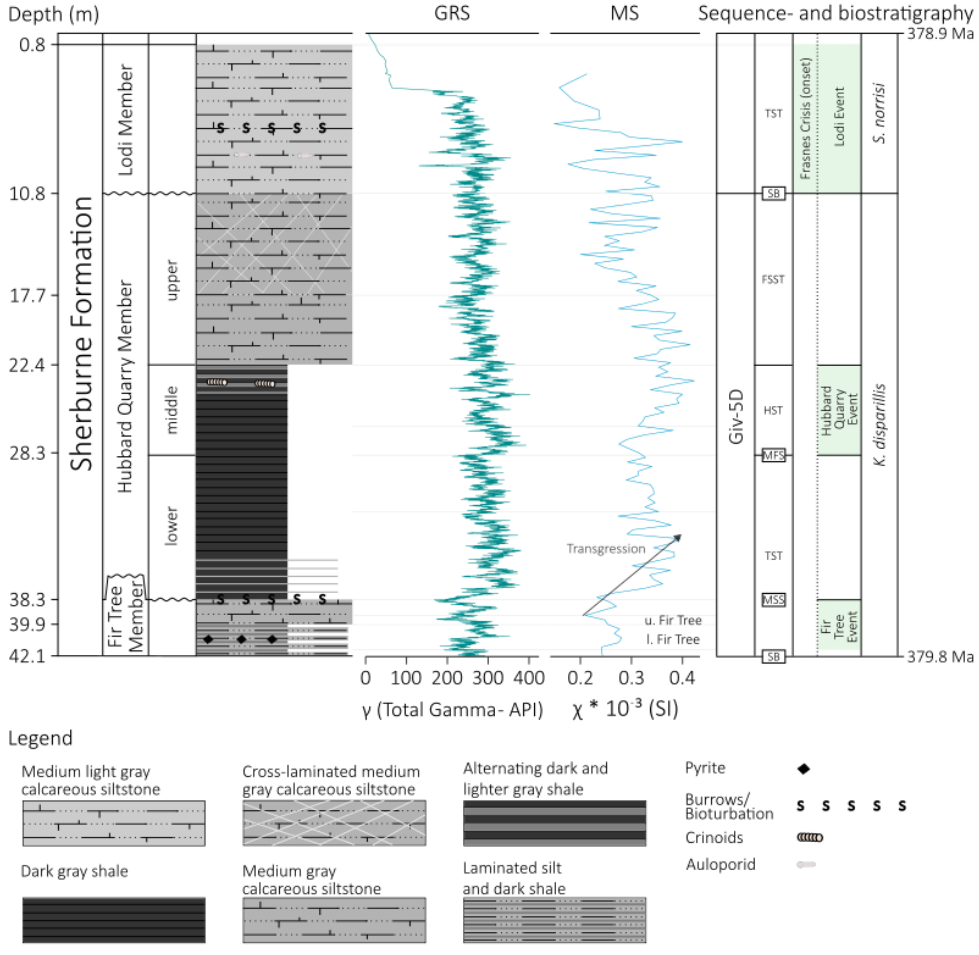

Fig. 2. Integrated stratigraphy of the Sherburne Formation in the Cargill #17 Core. Stratigraphy, lithological column, gamma ray spectrometry (GRS, total gamma – API), magnetic susceptibility (MS, SI – Kappa * 10^{-3}), sequence stratigraphy; subsequence Giv-5D, sequence boundary (SB), maximum starvation surface (MSS), highstand systems tract (HST), falling stage systems tract (FSST), transgressive systems tract (TST) from Brett et al. (2011) and Baird et al. (2023), event stratigraphy, conodont zonation (Kirchgasser, 1994), and numerical ages based on the conodont zonation (Becker et al., 2020).

https://doi.org/10.5194/egusphere-2026-2034
Preprint. Discussion started: 27 May 2026

3. Materials and Methods

3.1. Gamma-ray Spectrometry

High-resolution gamma ray spectrometry (GRS) total gamma 'γ' (API units) was acquired at ± 0.013 m spacing using a Core Lab Instruments Gamma Logger at the Department of Geosciences at the University of Cincinnati (Ohio, USA). The γ-signal is proportional to the naturally occurring γ-radiation of the sample and integrates contributions primarily from ^{40}K, ^{232}Th and ^{238}U (Killeen, 2015). It represents an amalgamated signal dominated by ^{40}K (and to a lesser extent by ^{232}Th), typically associated with clay-rich, detrital material, and by ^{238}U, which is often enriched in organic-rich intervals. Across most of the Sherburne Formation, the γ-signal is a reliable proxy for detrital input, with minor organic contributions restricted mostly to dark gray shales of the lower and middle Hubbard Quarry members.

3.2. Magnetic Susceptibility

Magnetic susceptibility (MS; 'χ' in SI-units Kappa 10^{-3}) was measured at ± 0.3 m spacing using Beloit College's handheld Terraplus KT-10R v2 meter while the core was on loan at the University of Cincinnati. The χ-signal represents the degree of magnetization of a material in response to an applied external magnetic field, which is commonly dominated by paramagnetic and ferromagnetic minerals which are typically enriched in detrital fractions of sedimentary rocks (Ellwood et al., 2000). When primary, the χ-signal also serves as a proxy for detrital input (Da Silva et al., 2009; 2012; De Vleeschouwer et al., 2012).

3.3. Statistical Approaches

Data treatment and statistical testing were performed in R Studio (version 2025.05.0+496). Time series and spectral analyses used "Astrochron" (Meyers, 2014) and "WaverideR" (Arts, 2023). GRS γ- and MS χ-signals were linearly interpolated and detrended using the detrend() or noLow() functions. Power spectral density was estimated via the multi-taper method (MTM; Thomson, 1982; Meyers, 2012). Significance testing employed AR(1)

https://doi.org/10.5194/egusphere-2026-2034
Preprint. Discussion started: 27 May 2026

models with a Bonferroni correction at the 90 %, 95 %, and 99 % confidence levels, assuming an AR(1) process as the null hypothesis. Evolutive spectral analysis was carried out primarily using continuous wavelet transforms (CWT; Arts, 2023; Arts et al., 2024), suited for capturing both frequency and depth/time localization in non-stationary signals, across a range of cyclicities, though with limited frequency resolution. Normalized evolutive harmonic analysis (EHA) and evolutive power spectral analysis (EPSA) ('eha' function, Meyers et al., 2001) tracked spectral features through time, highlighting oscillation magnitude and frequency strength. Taner bandpass filters isolated components of interest. Hilbert transforms were applied to filtered signals to assess envelopes, allowing for assessment of amplitude modulation patterns. Focus was placed on amplitude modulation patterns of precession, obliquity and short eccentricity cycles by extracting higher-order cycles from the envelope of hierarchically shorter cycles. To avoid convoluted phrases, for example, SE(i) is used to denote the '100-kyr short eccentricity cycle, recovered indirectly (i.e., 'i') from the envelope of precession'.

TimeOpt, an inverse modeling approach designed primarily for the evaluation of eccentricity-related amplitude modulation and bundling, was used to estimate sedimentation rates. This method enables astronomical tuning by identifying an optimal sedimentation rate that simultaneously optimizes (i) amplitude modulation of precession (or short eccentricity) by eccentricity, and (ii) concentration of spectral power at target orbital frequencies (Meyers, 2015). An average climatic precession target frequency of 0.0525 kyr^{-1} (~19.1 kyr) was calculated based on estimates by Waltham (2015) at 380 Ma.

Nonlinear interactions were assessed using bicoherence analysis, a high-order spectral method capable of identifying quadratic phase coupling (Hasselmann et al., 1963; Kim and Powers, 1979; Hinich, 1982; Choudhury et al., 2008; Sullivan et al., 2023). This approach detects a third, new frequency that arises from Milankovitch combination tones; sum ($f_3 = f_1 + f_2$) and difference ($f_3 = f_1 - f_2$) tones (e.g., Hagelberg et al., 1991; von Dobeneck and Schmieder, 1999; Da Silva et al., 2018; Sullivan et al., 2023).

https://doi.org/10.5194/egusphere-2026-2034
Preprint. Discussion started: 27 May 2026

4. Results

4.1. Gamma-ray Spectrometry

The γ-values fluctuate between 200-350 API across the Sherburne Formation, except in the fragmented upper Lodi Member, which is excluded from further analysis. The lowest values occur in the laminated siltstones to shales and calcareous siltstones of the Fir Tree Member, oscillating strongly around a ~250 API baseline. A pronounced shift to higher γ-values marks the base of the overlying Hubbard Quarry Member at 38.3 m, followed by fluctuations around a slightly declining ~300 API baseline. The transition from the lower to middle Hubbard Quarry Member (28.3 m) is marked by the highest γ-values, reaching approximately 400 API (MSS; Fig. 2), after which values progressively decrease through the upper Hubbard Quarry Member. In the Lodi Member, γ-values fluctuate around 250-300 API (Fig. 2). Superimposed on these larger-scale trends are prominent 0.5-1.5 m bundles, in turn grouped into meter- to decameter-scale rhythmic packages.

4.2. Magnetic Susceptibility

The Fir Tree Member shows consistently low χ-values (~0.25 SI). A pronounced increase marks the transition to the overlying lower Hubbard Quarry Member, followed by a gradual decline toward the middle Hubbard Quarry Member (28.3 m; Fig. 2). χ-values rise again to ~0.40 SI near the base of the upper Hubbard Quarry Member, then decrease to ~0.20 SI in its middle portion. From the middle of the upper Hubbard Quarry Member into the overlying Lodi Member, χ-values display strongest variability, ranging from 0.2 to 0.4 SI in the middle part of the Lodi Member (Fig. 2). Similar to the γ-signal, meter- to decameter-scale rhythmicity is superimposed on these larger-scale trends in the χ-signal.

https://doi.org/10.5194/egusphere-2026-2034
Preprint. Discussion started: 27 May 2026

5. Cyclostratigraphy

5.1. Depth-domain Cyclostratigraphy

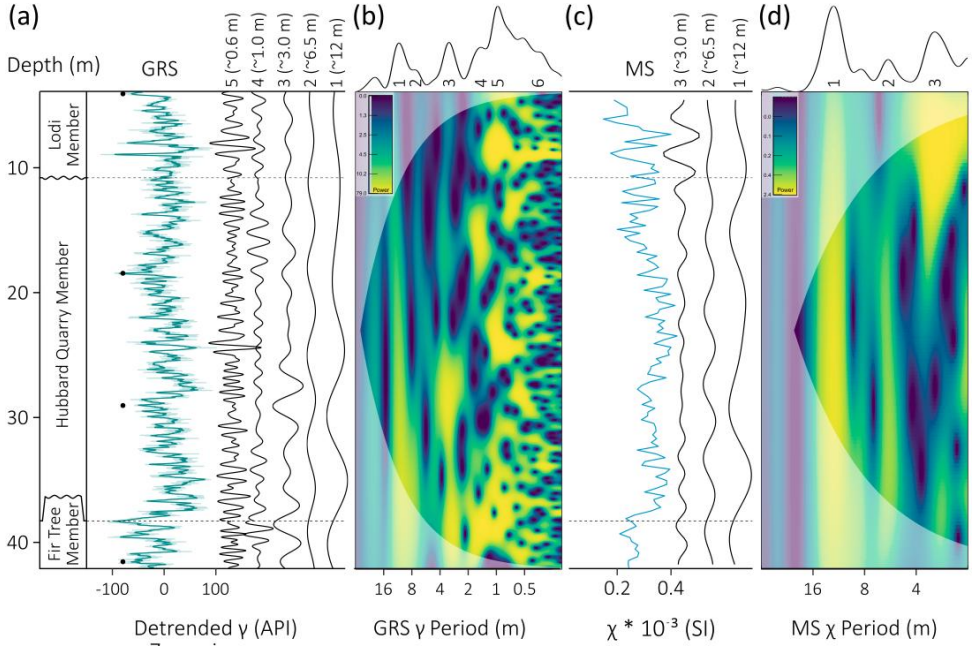

Fig. 3. Depth-domain cyclostratigraphy of the Sherburne Formation. a) Stratigraphy, detrended GRS γ-signal (light cyan) and 7-running average γ-signal (cyan), and bandpass filter output of key components 1 to 5 (black) and their corresponding mean periodicities (m). Components 3 to 5 were extracted separately for each member. Black dots indicate interpreted local minima in long-term cyclicity. b) GRS γ continuous wavelet transform and average wavelet power spectrum. c) MS χ-signal (blue) and bandpass filter output of key components 1 to 3 (black) and their corresponding mean periodicities (m). d) MS χ continuous wavelet transform and average wavelet power spectrum.

A CWT applied to the detrended γ-signal (Fig. 3a) reveals about six significant components exhibiting elevated wavelet power that appear significant versus 90 % AR(1) confidence level (MTM in Fig. S1). Although spectral power varies locally, mean periods remain relatively stable throughout the Sherburne Formation (Fig. 3b). Taner bandpass filtering extracted five components from the detrended γ-signal: 1 (~12 m), 2 (~6.5 m), 3 (~3.0 m), 4 (~1.0 m) and 5 (~0.6 m) (Fig. 3a). To account for minor mean frequency shift of

https://doi.org/10.5194/egusphere-2026-2034
Preprint. Discussion started: 27 May 2026

components 4 and 5, filtering was applied separately to each member, centering the window around intervals of highest spectral power. At the Fir Tree-Hubbard Quarry and Hubbard Quarry-Lodi contacts, a discrepancy in these components (Fig. 3) is interpreted as the expression of the minor discontinuities present (Baird et al., 2023).

A similar approach applied to the MS χ-signal (Fig. 3d) identified three key components with mean periodicities of ~12, ~6.5, ~3.0, and ~1 m. Of these, component 1 is statistically significant (90 % AR(1); Fig. S1). A fourth ~1.0-m component was also detected (Fig. S1) but excluded from interpretation due to low signal resolution. Taner bandpass filtering was used to extract three key signals (Fig. 3c).

https://doi.org/10.5194/egusphere-2026-2034
Preprint. Discussion started: 27 May 2026

5.2. *Cyclostratigraphic Age Models*

Milankovitch cycles are essential for constructing astronomical age models, and a key characteristic is their well-defined hierarchical structure, expressed through time-dependent frequency ratios. For the late Givetian (~380 Ma), average durations are: 405-kyr long eccentricity, 173-kyr long obliquity, ~100-kyr short eccentricity, 34.3-kyr obliquity, and ~19.1-kyr precession, yielding ratios of 1.0:1.8:5.2:9.1:21.2 that reflect their hierarchical structure. Components 1 to 5 in the γ-signal (Fig. 3b) exhibit ratios of 1.0:1.7:5.0:10.0:20.0, strongly suggesting the imprint of Milankovitch cyclicity. Similar periodicities in components 1 to 3 of the χ-signal further support this interpretation. Accordingly, the Sherburne Formation spans ~1.2 Myr at an average sedimentation rate of ~3 cm/kyr.

TimeOpt (0.2 to 4.0 cm/kyr; Meyers, 2015) was applied to test for amplitude modulation of precession by eccentricity and of short eccentricity by long eccentricity. For the γ-signal, average sedimentation rates of 3.29 and 3.39 cm/kyr were obtained, respectively (r^2opt; Fig. S2 and S3). In complement, TimeOpt testing for amplitude modulation of short eccentricity by long eccentricity, applied to the χ-signal, yielded an average sedimentation rate of 3.71 cm/kyr (r^2opt; Fig. S4). These estimates agree closely with the frequency-ratio estimates, strengthening the cyclostratigraphic interpretation. Conodont biostratigraphy (*K. disparilis* and *S. norrisi*; ~900 kyr; Becker et al., 2020) suggest comparable rates, well within the same order of magnitude (Fig. 2).

For the Late Givetian, the 405-kyr eccentricity 'metronome' remains the most stable and reliable Milankovitch cycle, even when considering the possibility that it could have been temporarily disrupted (Zeebe and Lantink, 2024). Accordingly, minimal tuning to the 405-kyr eccentricity was applied to the γ-signal (see black dots on Fig. 3a), guided by four local minima in the bandpass filter output of component 1 (Fig. 3b), interpreted to reflect 405-kyr long eccentricity. In the absence of an astronomical solution due to solar system chaos (Laskar, 2020), this approach provides the most reliable duration estimate. Using only four depth-time tie-points minimizes manipulation of the original γ-signal and preserves frequency modulation

https://doi.org/10.5194/egusphere-2026-2034
Preprint. Discussion started: 27 May 2026

(e.g., precession frequency modulation by eccentricity). This age model (hereafter AM1) yields a floating astrochronology ~1238 kyr and is ideal for investigating longer-term processes (~10^5 yr).

Recovery of all identified Milankovitch cycles (Fig. 3) from the time-domain γ-signal (Fig. 4) enabled a second, complementary tuning approach based on precession. Guided by the bandpass filter output of component 5 (Fig. 3a) and assuming a fixed 19.1-kyr precession period, a second age model (hereafter AM2) was constructed. The resulting floating astrochronology spans ~1267 kyr. Although the use of 67 depth-tie points at fixed 19.1-kyr intervals sacrifices information on the different frequency components of precession, this approach corrects more effectively for small-scale sedimentation rate variations. This is most crucial when investigating processes on sub-Milankovitch timescales, for which such a high-resolution age model is most ideal.

Finally, the estimated duration of the Cargill #17 Core Sherburne Formation is calculated by averaging AM1 and AM2, yielding 1252 ± 29 kyr (Fig. S5). The uncertainty associated with this estimate reflects the difference in relative time between AM1 and AM2 and is a realistic error margin equivalent to nearly two precession cycles. Both γ- and χ-signals were tuned using both AM1 and AM2 prior to subsequent cyclostratigraphic analysis.

https://doi.org/10.5194/egusphere-2026-2034
Preprint. Discussion started: 27 May 2026

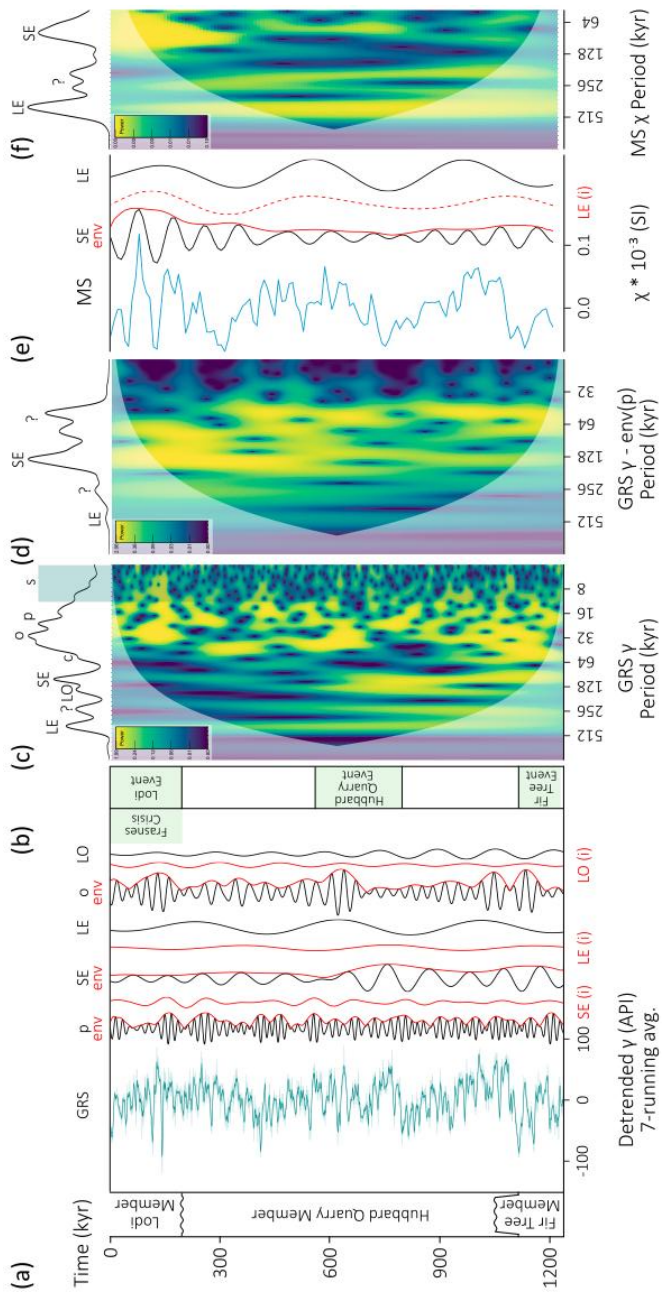

Fig. 4. Time-domain (AM1) cyclostratigraphy of the Sherburne Formation. a) Stratigraphy, detrended GRS γ-signal (light cyan) and 7-running average γ-signal (cyan), and bandpass filter output of precession (p; black) and its envelope (red), short eccentricity (SE; black) extracted from the envelope of precession (SE(i); red), short eccentricity (SE; black) and its envelope (red), long eccentricity extracted from the envelope of short eccentricity (LE(i); red), long eccentricity (LE; black), obliquity (o; black) and its envelope (red), long obliquity extracted from the envelope of obliquity (LO(i); red), long obliquity (LO; black). b) Bio-event stratigraphy. c) GRS γ CWT and average wavelet power spectrum, combination tones (c), and sub-Milankovitch cyclicity (s) highlighted in light blue. d) GRS γ CWT of the envelope of precession and average wavelet power spectrum. e) MS χ-signal (blue) and bandpass filter output of short eccentricity (SE; black) and its envelope (red), long eccentricity extracted from the short eccentricity envelope (LE(i); dashed red), long eccentricity (black). f) MS χ CWT and average wavelet power spectrum.

https://doi.org/10.5194/egusphere-2026-2034
Preprint. Discussion started: 27 May 2026

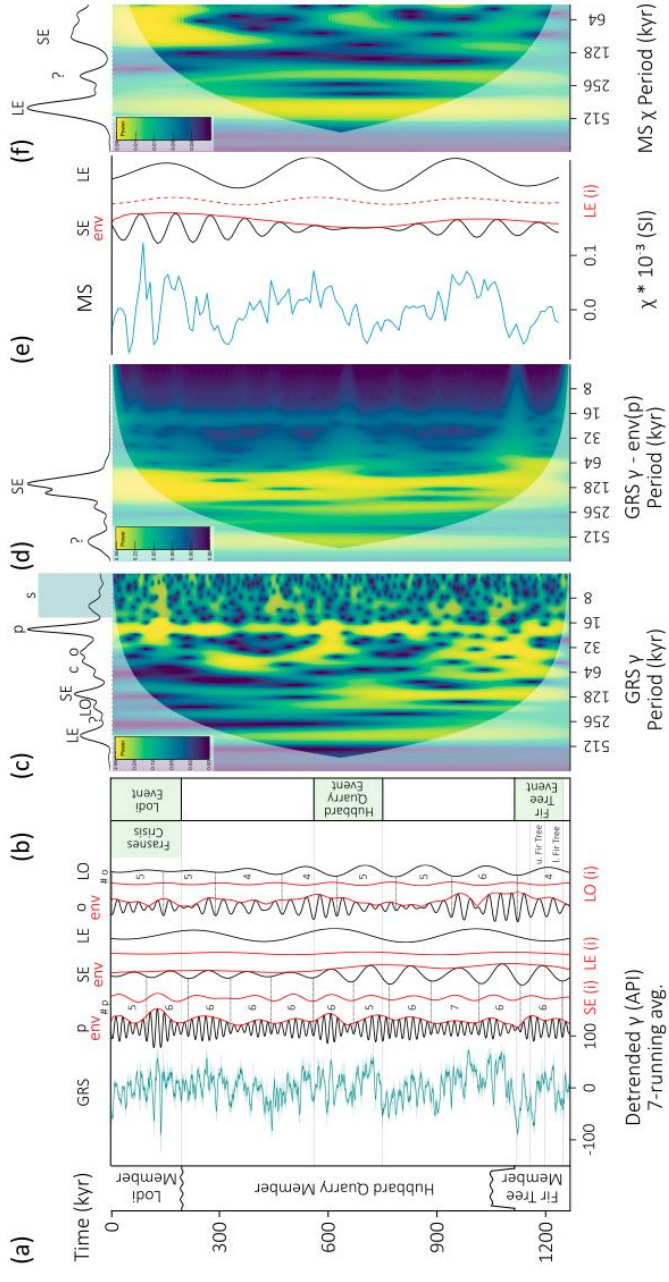

Fig. 5. Time-domain (AM2) cyclostratigraphy of the Sherburne Formation. a) Stratigraphy, detrended GRS γ-signal (light cyan) and 7-running average γ-signal (cyan), and bandpass filter output of precession (p; black) and its envelope (red), short eccentricity (SE; black) extracted from the envelope of precession (SE(i); red), short eccentricity (SE; black) and its envelope (red), long eccentricity extracted from the envelope of short eccentricity (LE(i); red), long eccentricity (LE; black), obliquity (o; black) and its envelope (red), long obliquity extracted from the envelope of obliquity (LO(i); red), long obliquity (LO; black). Numbers indicate counted precession (# p) cycles per interpreted SE cycle and obliquity (# o) per interpreted LO cycle. b) Bio-event stratigraphy. c) GRS γ CWT and average wavelet power spectrum, sub-Milankovitch cyclicity (s) highlighted in light blue. d) GRS γ CWT of the envelope of precession and average wavelet power spectrum. e) MS χ-signal (blue) and bandpass filter output of short eccentricity (SE; black) and its envelope (red), long eccentricity extracted from the short eccentricity envelope (LE(i); dashed red), long eccentricity (black). f) MS χ CWT and average wavelet power spectrum.

https://doi.org/10.5194/egusphere-2026-2034
Preprint. Discussion started: 27 May 2026

5.3. *Time-domain Cyclostratigraphy*

The Devonian lies beyond the interval for which astronomical solutions remain reliable, as chaotic divergence limits the precision of deep-time orbital calculations (Laskar, 2020; Zeebe and Lantink, 2024). We therefore assess the Milankovitch imprint through time-series and spectral analyses of the GRS γ- and MS χ-signals, tuned using two complementary age models: AM1 (405-kyr eccentricity) and AM2 (19.1-kyr precession). Both age models offer specific advantages and limitations that complement one another. Due to the long-term stability of the 405-kyr LE cycle, AM1 provides the most accurate temporal estimation and preserves frequency modulation, but it performs poorly in correcting for high-frequency sedimentation rate changes. In contrast, AM2 offers the highest temporal resolution and effectively accounts for sedimentation rate changes – thereby also more faithfully capturing amplitude modulation patterns – though it sacrifices precession frequency modulation. Consequently, while analyses targeting the linear Milankovitch imprint should yield comparable results across both models, higher-order spectral methods (e.g., bicoherence analysis) may produce divergent outputs, as they are more sensitive to phase structure and nonlinear interactions, whose detection can be affected by the tuning.

5.3.1. *Long Eccentricity-based Age Model (AM1)*

CWT analysis of the γ-signal tuned to AM1 reveals imprints of 405-kyr long eccentricity (LE), as well as ~173-kyr long obliquity (LO), ~100-kyr short eccentricity (SE), obliquity and precession cycles (Fig. 4c). These Milankovitch components were filtered, and their amplitude modulation (i.e., envelope) was obtained via Hilbert transform. About 5 to 7 precession cycles occur per short eccentricity cycle (Fig. 4a), matching predictions for the late Givetian (~380 Ma; Waltham, 2015). The amplitude modulation patterns of precession align satisfactorily with SE extrema. A second CWT of the precession envelope (Fig. 4d) shows dominant SE power, with only minor LE power, as expected for such a relatively short record (~3 LE cycles).

https://doi.org/10.5194/egusphere-2026-2034
Preprint. Discussion started: 27 May 2026

Sub-Milankovitch spectral power (s; Fig. 4c) suggests half-precession cycles and/or high-frequency combination tones (i.e., millennial-scale variability), statistically significant at the 90 % AR1 level (MTM; Fig 6a, Fig. S1c, d). Additional wavelet power appears between 35-65 kyr periods (Fig. 4c), which is also present in the envelope of precession (Fig. 4d) and half-precession, as shown later. These may reflect localized sedimentation rate changes, linear Milankovitch interferences (affecting the envelope of precession) or nonlinear interactions.

To explore the origin of cyclic components that deviate from canonical Milankovitch frequencies, bicoherence analysis was performed, with a focus on nonlinear interactions between precession and obliquity (Fig. 6c). In several regions of the spectrum, quadratic coupling between precession and obliquity is evident, producing sum tones (10.3 to 13.9 kyr) and/or difference tones (~36 to 128 kyr). Additional coupling occurs between sub-Milankovitch components and precession and obliquity components (Fig. 6c).

5.3.2. Precession-based Age Model (AM2)

Spectral analyses similar to those described in the previous section confirm LE, LO, SE and obliquity in addition to the precession cyclicity in the γ-signal that was tuned according to AM2 (i.e., precession-based; Fig. 5). This equally serves as a cross-check of the proposed cyclostratigraphic interpretation. Precession counts consistently yield 5-7 cycles per SE cycle (Fig. 5a). Similarly, obliquity counts reveal 4-6 cycles per LO cycle (Fig. 5a), equally in-line with astronomical predictions (~150 to 177 kyr in the ZB23 solutions; Zeebe and Lantink, 2024). These counts suggest the Fir Tree-Hubbard Quarry discontinuity represents only a minor hiatus, most likely shorter than one obliquity cycle. Similarly, the sequence boundary (SB) at the base of the Lodi Member also appears to represent only a minor hiatus of about the same duration. From this SB onwards, the precession envelope shifts slightly out of phase with the extracted SE cycle, possibly reflecting either the influence of the hiatus, edge effects introduced by bandpass filtering and subsequent Hilbert transform, or a change in the paleoclimatic response. A similar but weaker effect occurs in the lower Fir Tree Member. Conversely, the envelope of obliquity and LO does exhibit a consistent anti-phased

https://doi.org/10.5194/egusphere-2026-2034
Preprint. Discussion started: 27 May 2026

404 relationship, which may in part be due to the tendency of bandpass filtering and the Hilbert
405 transform to impose smoother, more regular phase behavior when signal amplitudes are low
406 (Fig. 4a, Fig. 5a).

407 Tuning to 19.1-kyr precession enhances sub-Milankovitch power (Fig. 5c), suggesting
408 half-precession and/or nonlinear interactions. Bicoherence analysis reveals strong diagonal
409 coupling at 19.1 kyr (Fig. 6d), consistent with (mathematical) harmonic generation producing
410 a ~9.55 kyr component. Quadratic coupling between precession and this component in turn
411 yields a ~6.37-kyr component, suggesting involvement of a harmonic cascade. Tuning to
412 precession can generate a harmonic cascade as an artefact, because it forces variations in
413 the sedimentation rate that effectively result in frequency modulation of the signal. However,
414 we observe that a ~9.55-kyr component is recovered through spectral analysis (Fig. 4) and it
415 also appears on the bicoherence spectrum of the γ-signal tuned according to AM1 (Fig. 6c),
416 where it couples with precession and obliquity components. This strongly suggests that the
417 detected sub-Milankovitch cyclicity (incl. the ~9.55-kyr component) is not only a tuning artifact
418 (Fig. 8).

419 *5.3.3. Magnetic Susceptibility*

420 Spectral and time series analyses of the χ-signal tuned to AM1 and AM2 yield highly
421 similar results and are therefore treated together. CWT analysis shows increased wavelet
422 power at LE and SE periodicities (Fig. 4), which are extracted using Taner bandpass filtering
423 (Fig. 4) to facilitate comparison of phase relationship between γ and χ. Crucially, the extracted
424 SE and LE components appear broadly in-phase with those recovered from the γ-signal (Fig.
425 4, 5), indicating that both proxies exhibit a similar response to astronomically forced insolation
426 changes. This reinforces their interpretation as reflecting detrital input variations.

https://doi.org/10.5194/egusphere-2026-2034
Preprint. Discussion started: 27 May 2026

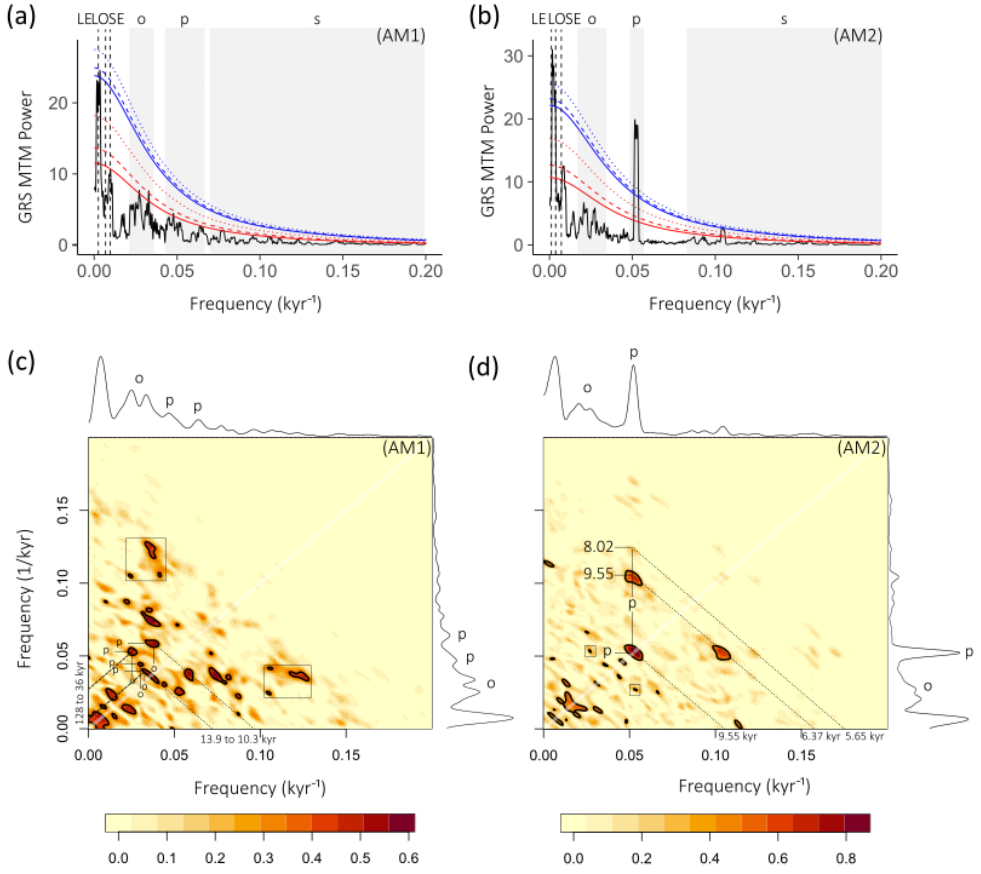

Fig. 6. Bicoherence analysis of the tuned GRS γ-signal. a) Time-domain γ (AM1) MTM spectrum. b) Time-domain γ (AM2) MTM spectrum. Classical significance testing at 90, 95 and 99 % confidence levels using an autoregressive model of order 1 (AR(1)) is included for each spectrum (red full, dashed and dotted red lines, respectively) and Bonferroni corrections (blue). c) Weighted overlap segment averaging (WOSA) power spectrum and bicoherence spectrum of γ (AM1). Obliquity and precession marked by 'o' and 'p', respectively. Increased bicoherence indicates quadratic coupling, revealing nonlinear Milankovitch combination (dotted diagonals) and difference (dashed diagonals) tones. Black squares indicate quadratic coupling of 9.55-kyr and sub-Milankovitch components. d) WOSA and bicoherence spectra of γ (AM2), black squares indicate regions of precession-obliquity coupling. Obliquity and precession marked by 'o' and 'p', respectively. Nonlinear Milankovitch combination tones (dotted diagonals). Key sub-Milankovitch durations highlighted on the bicoherence spectrum in kyr.

https://doi.org/10.5194/egusphere-2026-2034
Preprint. Discussion started: 27 May 2026

5.3.4. *Phase Relationship of Proxies to Astronomical Forcing*

Interpretation of proxy dynamics and their phase relationships with astronomical forcing is critical for understanding proxy responses and assessing the timing of regional events relative to Milankovitch cycle extrema. Cyclostratigraphy of γ- and χ-signals demonstrates that deposition of the Sherburne Formation strata within the Appalachian Basin was strongly influenced by astronomically paced changes in detrital input. Because both proxies represent an amalgamated signal (e.g., Da Silva et al., 2009; 2012; Killeen, 2015), it remains uncertain whether these variations represent changes in the total amount of detrital input or its composition. The dominant driver is most plausibly the hydrological cycle, influencing detrital delivery through variations in weathering, erosion, runoff, and/or astronomically paced eustatic sea-level fluctuations (Da Silva et al., 2009; 2012; Zhang et al., 2022). This is in agreement with the interpretation of the Sherburne Formation strata as hyperpycnites (Wilson and Schieber, 2014; 2015; 2017).

Intervals characterized by stronger γ precession-scale amplitude variation are interpreted to correspond to maxima in SE (Fig. 4, 5). The in-phase relationship between eccentricity signals extracted from both γ and χ indicates that both proxies respond synchronously to changes in insolation forcing. This is reinforced by the in-phase relationship between SE and SE(i) extracted from the γ-signal, suggesting maximal precession amplitude modulation during SE maxima (Fig. 4, 5). Accordingly, high γ- and χ-values are interpreted to reflect periods of strong climatic precession at the paleodepositional site. Similarities in proxy responses suggest that shared processes influenced χ in the same way, although its lower resolution limits detailed analysis. Although a 405-kyr LE imprint is recognizable in both proxy signals, its expression is less clear in the precession envelopes (Fig. 4, 5). This is attributed primarily to the presence of obliquity, combination tones (Fig. 6) and interferences involving precession and obliquity (Fig. 7), which affect the amplitude of the γ-signal and may hamper indirect recovery of eccentricity cycles from the envelopes of hierarchically shorter cycles.

https://doi.org/10.5194/egusphere-2026-2034
Preprint. Discussion started: 27 May 2026

5.3.5. *Duration of Regional Events and their Phase-relationship to Astronomical Forcing*

The durations of the Fir Tree, Hubbard Quarry, and Lodi events can be estimated with age model AM1, tuned to the stable 405-kyr eccentricity metronome. The Fir Tree Event lasted 108 ± 29 kyr, broadly equivalent to the duration of one short eccentricity cycle. The error margin of 29 kyr is estimated based on the difference between AM1 and AM2. The succeeding Hubbard Quarry Event, representing highstand conditions and associated low oxygen conditions inferred from the black shale facies (Fig. 2), is more protracted; its duration is 214 ± 29 kyr, equivalent to two SE cycles. Finally, the Lodi Event, which also marks the onset of the Frasnes Crisis, has an estimated duration of at least 200 ± 29 kyr.

The Fir Tree, Hubbard Quarry and Lodi events share a notable similarity: their onset occurs near a minimum in precession and short eccentricity (Fig. 5). Although this pattern is not explicitly diagnostic of the underlying causal mechanisms, it does indicate that astronomical forcing exerted a strong control on the timing of their initiation. Based on the 405-kyr long eccentricity cycle extracted directly from the γ- and χ-signals, the temporal position of these events can be placed within the broader long-eccentricity framework. Both the Fir Tree and Hubbard Quarry events appear to occur shortly after a minimum in 405-kyr eccentricity, initiating on the rising limb of the long-eccentricity cycle. Conversely, the Lodi Event appears to occur shortly after a maximum in 405-kyr eccentricity and unfolds of the decreasing limb of the long-eccentricity cycle.

Yet, while the Lodi and Fir Tree events are both interpreted to occur during a TST after a SB, the hypoxic Hubbard Quarry Event develops during a HST (Fig. 2). These differences – closely tied to eustatic sea-level variations – cannot be entirely reconciled with the eccentricity-paced forcing identified above. Although the timing of these events appears dictated by precession-eccentricity minima, their expression and relationship to sea-level variations likely involved additional controls. Given that the three events occur over slightly more than 1.2 Myr, we hypothesize that the s_4-s_3 1.2-Myr obliquity cycle (Laskar, 2020) may represent the additional pacing mechanism required to explain their differing sea-level contexts.

https://doi.org/10.5194/egusphere-2026-2034
Preprint. Discussion started: 27 May 2026

Astronomically controlled sea-level variability on such timescales was already reported by Huygh et al. (2026) for the Appalachian Basin during the Frasnian. Although the Sherburne Formation record is too short to resolve the s_4-s_3 cycle directly, the spacing of the Fir Tree, Hubbard Quarry and Lodi events is consistent with their development near successive extrema of this long-period obliquity modulation.

Whether the Fir Tree and Lodi event occur during a s_4-s_3 minimum or maximum – and, conversely, whether the Hubbard quarry corresponds to the opposite extremum – cannot be inferred from the available data. This uncertainty arises because the phase relationship between obliquity and sea-level change is mechanism-dependent: glacio-eustasy and limno/aquifer-eustasy respond in opposite phase to obliquity forcing (Lourens and Hilgen, 1997; Li et al., 2018), and the dominant mechanism depends on the prevailing climatic regime. Although the presence of substantial (continental) ice during the cooler Givetian (Becker et al., 2020) remains debated, integrated stratigraphy and oxygen-isotope evidence does suggest that glacio-eustatic processes may have operated on < 1.7-Myr timescales (Elrick et al., 2009). Hence, we propose that glacio-eustasy may have contributed to the observed eustatic sea-level variations. As noted above, the Fir Tree and Lodi events correspond with substantial incision of up to 18 meters in Iowa that is difficult to explain without glacio-eustasy, which could be substantial under relatively cool and variable climate conditions (cf. Dahl et al., 2022). Taken together, we hypothesize that obliquity-scale climate variability modulated the sea-level context in which the Fir Tree, Hubbard Quarry and Lodi events unfolded, superimposed on their precession-eccentricity-paced timing.

https://doi.org/10.5194/egusphere-2026-2034
Preprint. Discussion started: 27 May 2026

5.3.6. *Milankovitch Interference Patterns and Nonlinearities*

Insolation at a given latitude depends, among other factors (e.g., solar cycles), on climatic precession and obliquity (e.g., Milankovitch, 1941; Berger et al., 2006). Because different paleodepositional settings and proxies can respond to these orbital cycles through distinct mechanisms, their interplay may be recorded in multiple ways. Within the scope of this study, two types of interactions between astronomical frequencies are therefore relevant for understanding climate responses to insolation forcing.

The first involves linear interference between carrier frequencies such as precession and obliquity, which does not generate new frequencies in the underlying forcing (Fig. 8a, c; Laskar et al., 2004). Because precession and obliquity are not phase-locked, their extrema may coincide regularly but not periodically, and their combined linear effect generates time-dependent interference patterns manifested as amplitude modulation and beating patterns (Fig. 8b, d). The resulting amplitude envelope – extractable using a Hilbert transform (Fig. 8a, c) – contains frequency variability associated with the modulation itself (i.e., new frequencies; Fig. 8b, d). Depending on the sensitivity of the proxy system, a purely linear response may therefore record either the carrier frequencies and/or the amplitude envelope produced by their interference (Imbrie and Imbrie, 1980; Meyers and Hinnov, 2010). For completeness, certain processes, such as bioturbation, may mimic an envelope-type response (Meyers, 2014).

A second class of interactions involves nonlinear responses to astronomical forcing, leading the Earth system to generate new frequencies that are not present in the original insolation signal. Such behavior can occur in a range of contexts, including threshold-controlled climate-sediment interactions such as runoff-driven erosion and sediment accumulation (Tucker and Slingerland, 1997) as well as nonlinear sediment-transport dynamics (Jerolmack and Paola, 2010). This is conceptually illustrated in Fig. 8e, where a hyperbolic tangent $f(x) = \tanh[2(x-1)]$ acts as a nonlinear operator that produces mixed frequencies ($f_3 = f_1 \pm f_2$), such as ~50-kyr components (see Fig. 8f, g). Note that processes

https://doi.org/10.5194/egusphere-2026-2034
Preprint. Discussion started: 27 May 2026

that appear to track the amplitude envelopes of higher-frequency carriers may also be nonlinear in their underlying dynamics (e.g., Huybers and Wunsch, 2004). Quantifying the linear proxy response to the envelope of the carrier frequencies (e.g., to total insolation variability) and a nonlinear proxy response in inherently noisy sedimentary proxy series is challenging, especially because neither amplitudes nor frequencies are entirely diagnostic.

The framework presented above clarifies how new frequency components – such as those observed in the Sherburne Formation γ-signal – may arise and provides the basis for a qualitative interpretation of their origin. For example, a ~50-kyr component is present in obliquity (Laskar et al., 2004), but it is relatively weak and is not expected to contribute substantially (Spiering et al., 2024). Alternatively, such a component (Fig. 4-6) can result either from a linear response to the amplitude envelope of higher-frequency insolation components (Fig. 8d) or from nonlinear interactions involving, for example, precession and obliquity (Fig. 8g). A third possibility is that these components represent harmonics of the ~100-kyr short-eccentricity cycle. However, this pathway is readily evaluated: in the Sherburne Formation γ-signal, the extracted short-eccentricity component shows no stable phase relationship with the 40-60 kyr variability (Fig. S6), making a harmonic origin unlikely (Spiering et al., 2024). Moreover, this framework also highlights the limitations of time-series and spectral analysis in elucidating a proxy response to climatic variability as a result of insolation forcing. Although new frequency components arising from a response to the insolation envelope may exhibit higher amplitudes than those generated through nonlinear interactions (Fig. 8d, f), the amplitudes preserved in sedimentary proxy series may be muted, amplified, or overprinted by noise and other non-cyclic contributions (Mudelsee, 2010; Meyers, 2014), complicating their interpretation.

https://doi.org/10.5194/egusphere-2026-2034
Preprint. Discussion started: 27 May 2026

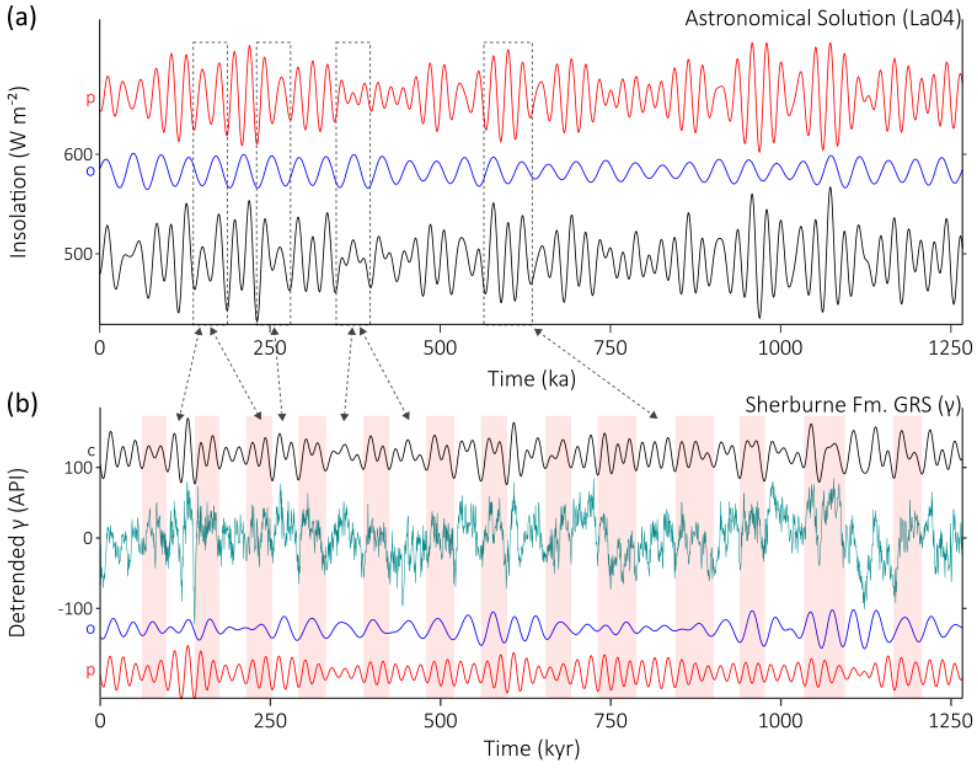

Fig. 7. Milankovitch interference patterns in the Sherburne Formation γ-signal. a) Insolation series (La04 at 65°N; Laskar et al., 2004) from 0 to 1267 ka (black), filtered precession (p; red) and obliquity (o; blue). Red bands and black dashed arrows highlight and indicate similar precession-obliquity interference patterns – not correlation. b) Detrended γ-signal (cyan) tuned according to AM2 and bandpass filter output of precession (p; red), obliquity (o; blue) and a linear superposition (i.e., sum) of the precession and obliquity filter output (c; black). Vertical red bars highlight interference patterns between precession and obliquity. Black dashed boxes and arrows indicate similar interference patterns.

https://doi.org/10.5194/egusphere-2026-2034
Preprint. Discussion started: 27 May 2026

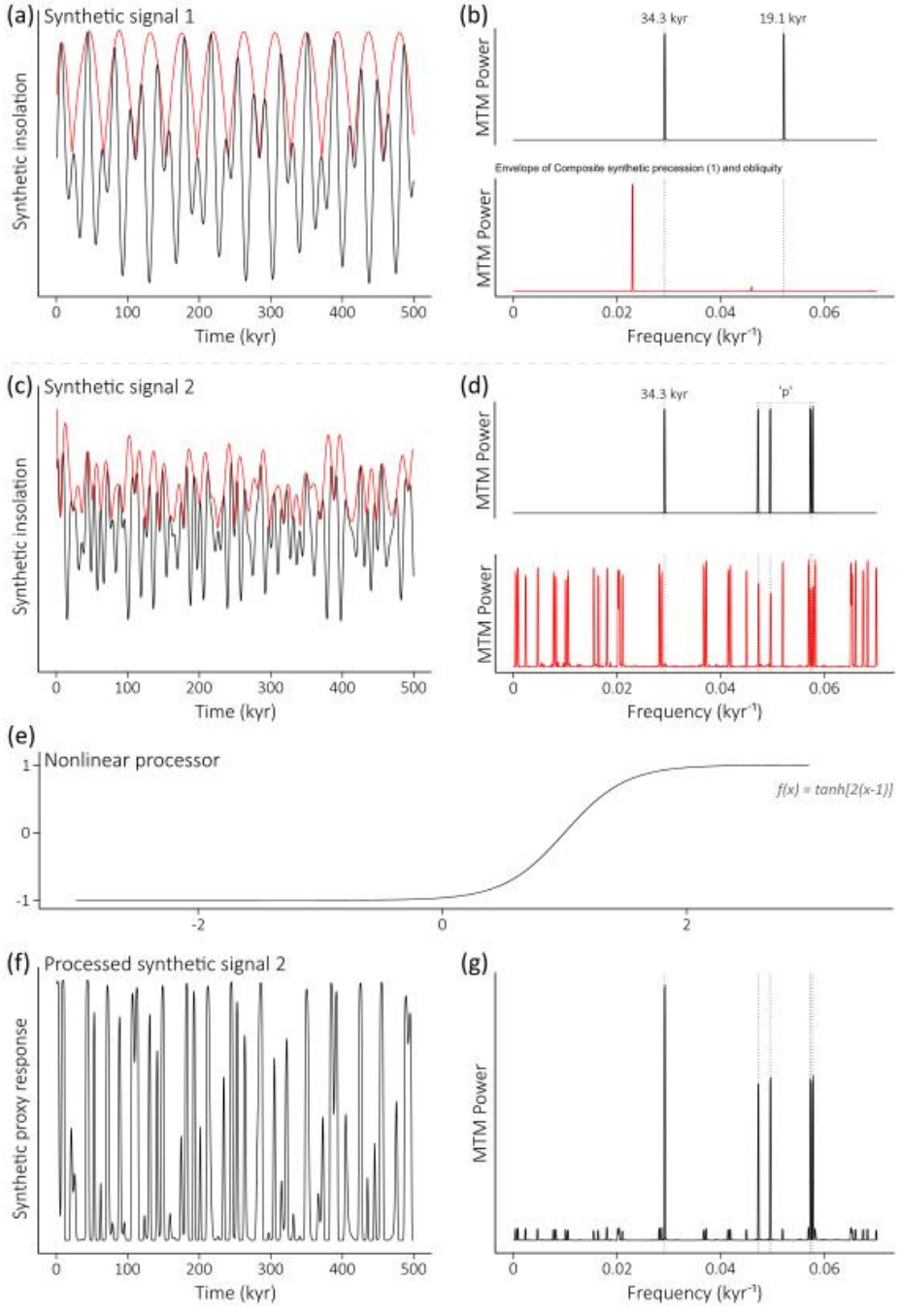

570

https://doi.org/10.5194/egusphere-2026-2034
Preprint. Discussion started: 27 May 2026

Fig. 8. Conceptual illustration of synthetic insolation forcing, proxy responses, and their MTM spectra. a) Synthetic insolation of linearly superimposed 19.1 and 34.3-kyr signals (black) and Hilbert-derived envelope (red), zoom-in on 0-500 kyr. b) MTM power spectra of the signals in a); upper: synthetic insolation (black), lower; its envelope (red). c) Synthetic insolation of linearly superimposed 17.34, 17.47, 20.2, 21.2 and 34.3-kyr signals (black) and Hilbert-derived envelope (red), zoom-in on 0-500 kyr. b) MTM power spectra of the signals in d); upper: synthetic insolation (black), lower; its envelope (red). e) nonlinear processor $f(x) = tanh[2(x-1)]$. f) Synthetic proxy response after nonlinear processing using $f(x) = tanh[2(x-1)]$ of the time series plotted in panel e. g) MTM power spectrum of the synthetic proxy response (f). Note that the prominence of envelope-derived or nonlinear frequency components is sensitive to the chosen input parameters of the conceptual experiment.

Building on this framework, the cyclicity observed in the Sherburne Formation γ-signal is interpreted here as reflecting a nonlinear proxy response to climatic variability with substantial contributions from a linear response to insolation and its envelope. Integration of bandpass filtering (Fig. 3, 4, 5, 7) with CWT (Fig. 4, 5) and bicoherence analysis (Fig. 6) supports this dual-mechanism interpretation. Apparent interference patterns, resulting from linear superposition of precession and obliquity appear to dominate the γ-signal (Fig. 7) and reflect a response to changes in total insolation (Laskar et al., 2004). The similarity between these precession-obliquity interference patterns and the La04 solution (Fig. 7a) is highly suggestive of a dominant contribution by a linear proxy response to insolation variability. Because no unique astronomical solution exists for the Givetian, these interference patterns are compared with the La04 insolation series for illustration purposes (from 0 to 1267 ka; Laskar et al., 2004; Fig. 7). Note that direct comparison may be somewhat limited due to the shorter Givetian precession and obliquity durations (Laskar et al., 2004; Waltham, 2015; Laskar, 2020).

In addition to these interference patterns, the Sherburne Formation γ-signal also exhibits features that cannot be produced by linear superposition alone; significant bicoherence between astronomical components (Fig. 6) demonstrates that the climate-sediment system introduces nonlinear interactions, generating new frequencies through

https://doi.org/10.5194/egusphere-2026-2034
Preprint. Discussion started: 27 May 2026

quadratic phase coupling (Sullivan et al., 2023) and likely further modifying the amplitude structure of the proxy response. Such nonlinear interactions may give rise to both lower-frequency (i.e., sum tones) and higher-frequency (i.e., difference tones) components (Hagelberg et al., 1991; von Dobeneck and Schmieder, 1999). Although nonlinear interactions can generate similar frequencies, for example, in the 40-60 kyr band (Fig. 6), climate-sediment nonlinearities are typically state-dependent and not expected to generate persistent, well-defined patterns (Tucker and Slingerland, 1997; Jerolmack and Paola, 2010) such as those arising from a response to total insolation variability (Fig. 7a, b). While bicoherence analysis does not allow discrimination between sum and difference tones, our integrated spectral (Fig. 4-7) and conceptual (Fig. 8) results indicate that both types of nonlinear products were likely captured by the γ-signal. Although additional cyclicity is evident at eccentricity timescales (Fig. 4-6), the summed precession-obliquity signal appears to account for the majority of variability observed in the γ-signal (Fig. 7), while non-cyclic contributions and sedimentary noise likely also contributed. The considerations outlined above are equally relevant for interpreting variability in the sub-Milankovitch band, where both half-precession and nonlinear frequency generation can produce similar spectral expressions, which is addressed in the next section.

https://doi.org/10.5194/egusphere-2026-2034
Preprint. Discussion started: 27 May 2026

5.3.7. *Half-precession Cycles*

In the intertropical belt, in particular at the equator, the Sun culminates at the zenith of both equinoxes (Berger et al., 2006). If climate responds predominantly to the largest of these twice-annual insolation maxima (Berger and Loutre, 1997), then the precessional modulation of equinox intensity produces two insolation peaks per precession cycle, giving rise to variability at approximately half the precession period (i.e., mean ~9.5 kyr for the Givetian). Thus, half-precession does not represent a harmonic of precession; rather, it is a geometric consequence of how equatorial insolation responds to climatic precession (Berger and Loutre, 1997; Berger et al., 2006; Wu et al., 2025). However, distinguishing half-precession is not straightforward, because nonlinear interactions between precession and obliquity (Fig. 6; Table E1) or a proxy response to the total-insolation envelope (Fig. 8d) can generate frequencies that fall within the same band, complicating the elucidation of a true half-precessional signal.

The γ-signal consistently shows splitting of precession-scale cycles (Fig. 9a), suggesting a half-precession-like imprint. In addition, the γ CWT spectra reveal prominent power centered around a ~9.5 kyr period (Fig. 4, 5). MTM and EPSA analyses (Fig. S7) show that this band comprises multiple components (7.8 to 12.3 kyr) across the Sherburne Formation (see MTM spectrum, Fig. S1). Moreover, elevated bicoherence (Fig. 6) suggests the presence of similar frequencies resulting from nonlinearities and their involvement in quadratic coupling.

https://doi.org/10.5194/egusphere-2026-2034
Preprint. Discussion started: 27 May 2026

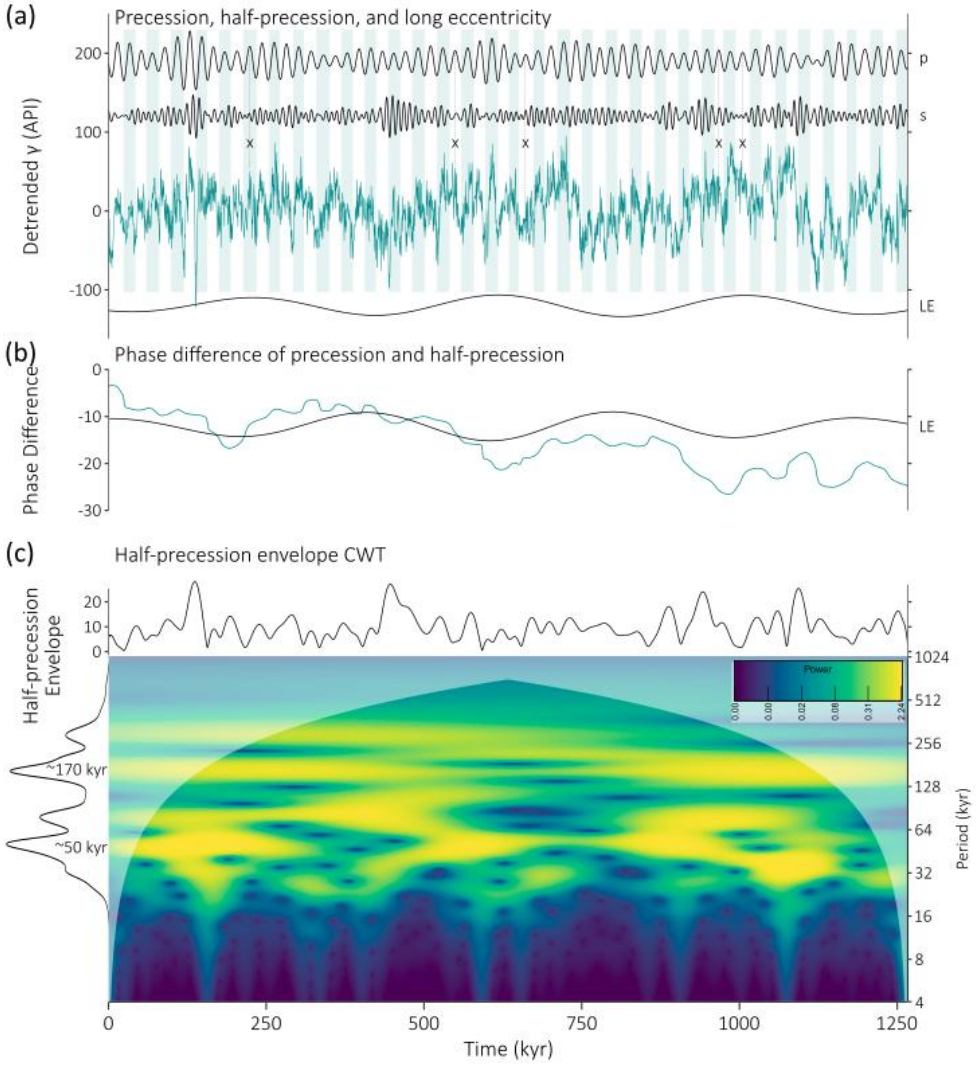

635

636 **Fig. 9. Half-precession cyclicity in the Sherburne Formation γ-signal.** a) Detrended γ-signal (cyan) tuned
637 according to AM2 and bandpass filter output of ~9.5-kyr sub-Milankovitch 'half-precession' cycles (s; black),
638 precession (p; black) and 405-kyr long eccentricity (LE; black). Intervals where a 2:1 s:p-structure breaks down are
639 marked using 'x', for which dashed vertical lines demarcate the temporal location of interpreted half-precession
640 cycles. b) The phase difference between extracted precession and half-precession cycles (cyan) and filtered 405-
641 kyr component (LE; black). c) Half-precession envelope (black) and continuous wavelet spectrum of the half-
642 precession envelope revealing pronounced ~50-kyr and ~170-kyr cyclicity.

https://doi.org/10.5194/egusphere-2026-2034
Preprint. Discussion started: 27 May 2026

Using Taner bandpass filters, precession and the ~9.5-kyr sub-Milankovitch components were isolated from the γ-signal (AM2), enabling direct comparison of bundling patterns and phase coherency (Fig. 9). The robustness of the ~9.5-kyr bandpass filter was verified to exclude artefacts arising from filter-window parameters. Throughout the formation, two ~9.5-kyr cycles consistently occur per precession cycle (Fig. 9a). Only four intervals (~6 %) deviate from this 1:2 ratio, which may reflect localized sub-precession sedimentation-rate changes, sedimentary noise (e.g., traditional slope-derived turbidites) or, more likely, interference from combination tones (Fig. 6). Such tones are absent from the insolation spectrum (e.g., Laskar et al., 2004) and instead reflect state-dependent climate-sediment feedbacks (Hagelberg et al., 1991; Tucker and Slingerland, 1997; Jerolmack and Paola, 2010), rather than a consistent half-precession response. The persistent ~9.5-kyr frequencies (Fig. 6; Fig. S7) and repeated two-per-precession bundling (Fig. 9a) strongly suggest half-precession cyclicity as the dominant source of sub-Milankovitch variability, with secondary contributions from nonlinear interactions. Therefore, while the identified ~9.5-kyr components cannot be interpreted as reflecting half-precession alone, we consider half-precession to be the dominant contributor and use this term as shorthand for this frequency band in the following discussion. Sub-7-kyr cyclicity is attributed to either Milankovitch combination tones or harmonics of (half-) precession (Fig. 6; Fig. S7). To further assess the relative contributions of half-precession and nonlinear sub-Milankovitch imprints, we examine the phase and amplitude modulation patterns of half-precession.

Visual inspection of the extracted precession and half-precession shows that their local extrema do not align, suggesting that the two signals are not phase locked. Such behavior is expected given the identified presence of nonlinearities (Fig. 6). To test this visual observation, the 1:2 phase-locking signal at a given time index *(t)* was calculated (Fig. 9b) using the instantaneous phases (using a Hilbert transform) of filtered precession and half-precession, according to:

$$\Delta\phi(t) = 2\phi_{pre}(t) - \phi_{hpre}(t) \quad (1)$$

https://doi.org/10.5194/egusphere-2026-2034
Preprint. Discussion started: 27 May 2026

where $\Delta\phi(t)$ represents the phase difference between the instantaneous phase of precession $\phi_{pre}(t)$ and 'half-precession' $\phi_{hpre}(t)$ (Rosenblum et al., 1996). The phase locking value (PLV) was calculated to quantify the consistency of the phase difference over (t), with values of 0 indicating random phase difference (i.e., no locking) and 1 indicating perfect phase locking:

$$PLV = \left|\frac{1}{N}\sum_{t=1}^{N} e^{i\Delta\phi(t)}\right| \quad (2)$$

where N represents the number of datapoints and the $e^{i\Delta\phi(t)}$ term expresses the phase difference as a unit-length complex vector (Lachaux et al., 1999). A PLV of ~0.28 indicates that the phase difference between precession and half-precession is not entirely random, but highly unstable. This behavior is illustrated in Fig. 9b, which shows a steadily decreasing baseline in $\Delta\phi(t)$ with a superimposed ~405-kyr fluctuation that strongly resembles long eccentricity and is consistently anti-phased to the 405-kyr LE extracted from the γ-signal (Fig. 9). From this, we infer that eccentricity influenced the phase evolution of precession and half-precession.

To further investigate the origin of sub-Milankovitch cyclicity, the envelope of the extracted half-precession, obtained through a Hilbert transform, was examined to assess the longer-period amplitude modulation of this band. A CWT shows that the resulting envelope is dominated by ~50-kyr and ~170-kyr variability. At first glance, this appears unexpected, because eccentricity modulates precession and one might therefore anticipate ~100-kyr (short eccentricity) and ~405 kyr (long eccentricity) modulation in the envelope of the half-precession signal. Such a ~170 kyr component is intriguing given it broadly corresponds to the s_3-s_6 "metronome" (Laskar, 2020), which has a periodicity of 150 to 177 kyr (Zeebe and Lantink, 2024) but, given that the 173-kyr component extracted from the γ-signal is relatively weak (Fig. 4, 5), we refrain from attempting to further interpret this feature.

https://doi.org/10.5194/egusphere-2026-2034
Preprint. Discussion started: 27 May 2026

6. Paleoclimatic and Paleodepositional Response

We now set insights obtained through cyclostratigraphic analysis of the Sherburne Formation γ- and χ-signals into a broader paleoclimatic perspective, providing new constraints on how astronomical forcing shaped the late Givetian paleoclimate and depositional processes in the Appalachian Basin. The cyclic variability points to a complex interplay among precession, obliquity, and eccentricity, reflecting a climate system responding to changes in total insolation, for example through precession-obliquity interferences, in combination with nonlinear climate-sediment interactions.

An obliquity imprint is – at first glance – somewhat surprising at a ~30° S paleolatitude because the direct effect of obliquity on insolation is strongest at high latitudes and is less pronounced near the equator (Milankovitch 1941, Berger et al., 1993, 2006; Laskar et al., 2004). Indeed, focusing on a Belgian record, De Vleeschouwer et al. (2012) suggested that the influence of high-latitude climate variability was very limited (or absent) at ~7°S paleolatitude during the Middle Devonian. Yet, the detected combination tones involving obliquity (Fig. 6) and the clear precession-obliquity interference patterns in the γ-signal (Fig. 7A) unmistakably reaffirm the imprint of obliquity on the Sherburne Formation γ-signal, identified through spectral analysis (Fig. 4, 5). This suggests that obliquity was also transmitted into the subtropics through climate-system pathways – rather than direct insolation forcing alone – consistent with a dynamically coupled tropical-subtropical climate system. Dynamic variations of, for example, the Intertropical Convergence Zone (ITCZ) net precipitation (De Vleeschouwer et al., 2012) are expected to respond to both precession and obliquity, which modulate seasonal and annual-mean temperature gradients, respectively (Schneider et al., 2014). This interplay between tropical hydrology and higher-latitude forcing is consistent with modeling results of Tuenter et al. (2003), who demonstrated – for the modern African summer monsoon – that obliquity-driven high-latitude climate variability can be transmitted into the tropics and subtropics through large-scale atmospheric circulation. Moreover, Zhang et al. (2022) reported combined precession and obliquity forced ITCZ migration at 5-20°N during

https://doi.org/10.5194/egusphere-2026-2034
Preprint. Discussion started: 27 May 2026

the Early Cambrian as a result of interhemispheric pressure contrasts, thereby influencing the lower-latitude hydrological cycle.

Recovery of a relatively strong obliquity imprint could suggest climatic teleconnections from high latitudes (e.g., Meyers, 2012; Zeeden et al., 2019) involving changes in ice volume (c.f. De Vleeschouwer et al., 2014). Although direct evidence of continental ice during the Middle Devonian is absent, the potential presence of continental ice during this cooler interval (Becker et al., 2020) has long been pondered (Elrick et al., 2009; Dahl et al., 2022) and on eustatic sea-level fluctuations. Although a glacio-eustatic regime could strongly contribute to the amplification of obliquity, it should be stated that a relatively strong obliquity imprint does not *per se* reflect the presence of continental ice (Gérard et al., 2026). Moreover, Bosmans et al. (2015) reported that "*obliquity-induced changes in tropical climate can occur without high-latitude ice sheet fluctuations*" and that tropical circulation changes (in their climate model) are consistent with obliquity-induced changes in the cross-equatorial insolation gradient. The effect of changes in insolation on high-latitude productivity in combination with ocean circulation changes influenced by obliquity at higher latitudes (i.e., thermohaline circulation) offer alternative or additional explanations for the translation and amplification of obliquity at lower latitudes (Gérard et al., 2025; 2026). As currently reconstructed (Fig. 1), the paleogeography of the northern Appalachian Basin is restricted and therefore prone to ocean circulation changes (see Zambito et al., 2012, for discussion of circulation changes in the Sherburne-preceding Tully Formation). Ultimately, the Sherburne Formation record underscores that subtropical climate during the Middle Devonian was not isolated from high-latitude forcing, but dynamically linked via a combination of teleconnection, circulation dynamics and, potentially, ice-volume variability.

Half-precession is generally considered unique to equatorial insolation forcing (Berger and Loutre, 1997; Berger et al., 2006). Recovery of such frequencies from detrital influx at relatively high latitudes (~30° S) therefore suggests considerable interactions with tropical climate variability, likely mediated through the hydrological cycle (*cf.*, western equatorial

https://doi.org/10.5194/egusphere-2026-2034
Preprint. Discussion started: 27 May 2026

Pacific; Wu et al., 2025). During the Middle Devonian, one of the most potent drivers of hydrological cycle variability was the precession-forced monsoonal circulation over the Euramerican continent within the pantropical belt (De Vleeschouwer et al., 2012). Migration of the intertropical convergence zone (ITCZ) modulated monsoonal activity, producing wet-dry cycles that governed detrital input and composition (De Vleeschouwer et al., 2012; 2014; Zhang et al., 2022; Wichern et al., 2024). Yet, the Sherburne Formation was deposited at an estimated paleolatitude of ~30°S – potentially beyond the latitudinal range typically reached by the ITCZ. Although De Vleeschouwer et al. (2014) inferred a substantial southward ITCZ displacement toward the Appalachian Basin during the Late Devonian SH summer (see also Wichern et al., 2024), such migration was likely part of a broader dynamical framework. In particular, ITCZ position should be viewed in conjunction with Hadley-cell behavior, which governs the large-scale redistribution of heat and moisture across the tropics and subtropics (e.g., Bian et al., 2025). Given the sensitivity of the hydrological cycle to astronomical forcing, it is hypothesized that similar mechanisms contributed to amplification of half-precession at higher latitudes, alongside ocean-circulation-driven teleconnections (Wu et al., 2025). Fundamentally, climatic precession and half-precession cycles are both driven by eccentricity-modulated precession (Berger and Loutre, 1997; Berger et al., 2006). Even though two half-precession cycles occur per precession cycle (Berger et al., 2006), their insolation expression in terms of amplitude and phase may differ depending on latitude and geometry (e.g., Wu et al., 2025). This would, in addition to high-frequency sedimentation rate changes, and the presence of combination tones as a result of nonlinearities in the climate-sediment system, explain why the extracted half-precession cycles are not phase-locked with precession (Fig. 9). Additionally, climate simulations show that the presence of ice sheets can further modulate the amplitude and phase of half-precession responses by altering the background climate state (Wu et al., 2025). Together, these mechanisms offer an explanation that accounts for the modulated, non-phase-locked half-precession signal recovered from the Sherburne Formation.

https://doi.org/10.5194/egusphere-2026-2034
Preprint. Discussion started: 27 May 2026

7. Conclusions

The cyclostratigraphic framework developed for the Sherburne Formation, guided by the 405-kyr long-eccentricity metronome, reveals substantial astronomical forcing of detrital influx in the late Givetian Appalachian Basin at ~30°S. Our results support a precession-dominated hydrological regime with a distinct obliquity imprint and persistent half-precession cycles. Based on the recognized Milankovitch imprint, the new cyclostratigraphic age model constrains the duration of the Sherburne Formation in the Cargill #17 core to 1252 ± 29 kyr, and constrains the durations of the regional Fir Tree, Hubbard Quarry, and Lodi events to 108 ± 29 kyr, 214 ± 29 kyr, and at least 200 ± 29 kyr, respectively – consistent with one to two short eccentricity cycles. The onset of the global Frasnes Crisis unfolds during a 405-kyr long eccentricity maximum and, possibly, during an extremum of the 1.2-Myr s_4-s_3 obliquity-modulation cycle governing eustatic sea-level variations.

The recovery of half-precession and obliquity in the pantropical belt highlights a complex interplay of equatorial and high-latitude dynamics, shaping changing climatic conditions. Nonlinear climate-sediment dynamics further influenced how these astronomical rhythms were transmitted into the basin, affecting their expression in the detrital record. This interplay can be understood in terms of the broader climatic mechanisms at work: climatic teleconnections, monsoonal dynamics, ITCZ and Hadley-cell migration, ocean-circulation changes, and possibly glacio-eustasy, collectively exerted considerable control over the paleodepositional environment. Together, these mechanisms exerted strong control over sediment supply to the Appalachian Basin, underscoring the strong and complex influence of astronomical forcing on the late Givetian climate.

https://doi.org/10.5194/egusphere-2026-2034
Preprint. Discussion started: 27 May 2026

Conflict of Interest

The authors declare there are no conflicts of interest in this manuscript.

Acknowledgements

This is a contribution to the "Projet de Recherche" funded by the Belgian National Fund of Sciencific Research (FNRS), contract T.0037.22 "WarmAnoxia". Thomas J. Algeo is acknowledged for supervising the GRS measurements of the Cargill #17 Core at the University of Cincinnati, Ohio (USA) by Kyleigh Hope, A.J. Kmetz, and Thomas Gott. Magnetic susceptibility data collection was undertaken by Beloit College undergraduates May Willison and Olivia Farbarik; this work was supported by the donors of ACS Petroleum Research Fund under Undergraduate Research Grant 60525-UR2 to J. Zambito.

https://doi.org/10.5194/egusphere-2026-2034
Preprint. Discussion started: 27 May 2026

Author contributions

Jarno J.C. Huygh: Conceptualization, Data curation, Formal analysis, Investigation, Methodology, Validation, Visualization, Writing – original draft.

Carlton E. Brett: Funding acquisition, Investigation, Project administration, Resources, Supervision, Validation, Writing – review & editing.

James J. Zambito IV: Funding acquisition, Investigation, Project administration, Resources, Validation, Writing – review & editing.

Loïc Sablon: Conceptualization, Data curation, Formal analysis, Investigation, Methodology, Validation, Visualization, Writing – original draft.

Justin Gérard: Conceptualization, Investigation, Validation, Writing – review & editing.

Ian J. Forsythe: Data curation, Investigation, Supervision, Validation, Writing – review & editing.

Michel Crucifix: Conceptualization, Formal analysis, Funding acquisition, Investigation, Methodology, Project administration, Resources, Supervision, Validation, Writing – review & editing.

Anne-Christine Da Silva: Conceptualization, Formal analysis, Funding acquisition, Investigation, Methodology, Project administration, Resources, Supervision, Validation, Writing – review & editing.

Data and Code Availability Statement

All data and R-code can be found via 10.5281/zenodo.19483389

https://doi.org/10.5194/egusphere-2026-2034
Preprint. Discussion started: 27 May 2026

References

Arts, M. C. M., 2023. WaverideR: Extracting Signals from Wavelet Spectra. https://CRAN.R-project.org/package=WaverideR

Arts, M. C .M., Corradini, C., Pondrelli, M., Pas, D., Da Silva, A.-C., 2024. Age and orbital forcing in the upper Silurian Cellon section (Carnic Alps, Austria) uncovered using the WaverideR R package. Front. Earth Sci.; 12, https://doi.org/10.3389/feart.2024.1357751

Baird, G. C., Zambito, J. J. VI, Brett, C. E., 2023. Tully Formation and pre-Frasnian Genesee Group succession, 259-378, In: Devonian of New York, Volume 2: Lower to upper Givetian (Middle Devonian) stage, Ver Straeten, C. A., Over, D. J., Woodrow, D. (eds.), *Bull. Am. Paleontol.*; 405-406. https://doi.org/10.32857/bap.2023.405.03

Becker, R. T., Königshof, P., Brett, C. E., 2016. Devonian climate, sea level and evolutionary events: an introduction. In: Devonian climate, sea level and evolutionary events, Becker, R. T., Königshof, P., Brett, C. E. (eds.), *Geol. Soc. Lond., Spec. Publ.*, 423, 1-10.

Becker, R. T., Marshall, J. E. A., Da Silva, A.-C., 2020. The Devonian Period. In: Gradstein, F. M., Ogg, J. G., Schmitz, M. D. And Ogg, G. (eds.), *The Geologic Time Scale 2020*; chapter 22, 733-810. https://doi.org/10.1016/B978-0-12-824360-2.00022-X

Berger, A. L., 1987. Long-term variations of caloric insolation resulting from the Earth's orbital elements. *Quat. Res.*; 9, 139-167.

Berger, A. L., 1988. Milankovitch Theory and Climate. *Rev. Geophys.*; 26, 4, 624-657. https://doi.org/10.1029/RG026i004p00624

Berger, A., and Loutre, M.F., 1997. Intertropical latitudes and precessional and half-precessional cycles. *Science*; 278, 1476-1478.

Berger, A., Loutre, M.F., Mélice, J.L., 2006. Equatorial insolation: from precession harmonics to eccentricity frequencies. *Clim. Past*; 2, 131-136

Bian, J., Räisänen, J., and Seppä, H., 2025. Mid-Holocene Intertropical Convergence Zone migration: connection with Hadley cell dynamics and impacts on terrestrial hydroclimate. *Clim. Past*; 21, 7, 1209-1233. https://doi.org/10.5194/cp-21-1209-2025

Bosmans, J. H. C., Hilgen, F. J., Tuenter, E., Lourens, L. J., 2015. Obliquity forcing of low-latitude climate. *Clim. Past*; 11, 1335-1346. doi:10.5194/cp-11-1335-2015

Brett, C. E., Baird, G. C., Bartholomew, A. J., DeSantis, M. K., Ver Straeten, C. A., 2011. Sequence stratigraphy and a revised sea-level curve for the Middle Devonian of eastern North America. *Palaeogeogr. Palaeoclimatol. Palaeoecol.*; 304, 21-53. doi:10.1016/j.palaeo.2010.10.009

Brett, C. E., Zambito, J. J. IV, McLaughlin, P. I., Emsbo, P., 2020. Revised perspectives on Devonian biozonation and environmental volatility in the wake of recent time-scale revisions. *Palaeogeogr. Palaeoclimatol. Palaeoecol.*; 549, 108843. https://doi.org/10.1016/j.palaeo.2018.06.037.

Choudhury, S., Shah, S., Thornhill, N., 2008. Diagnosis of process nonlinearities and valve stiction: Data driven approaches, Chapter 3, 29-41. *Springer*, ISBN: 978-3-540-79223-9. doi:10.1007/978-3-540-79224-6

Copper, P., and Scotese, C. R., 200. Megareefs in Middle Devonian supergreenhouse climates, In: Chan, M. A., and Archer, A. W. (eds.), Extreme depositional environments: Mega end members in geologic time: Boulder, Colorado, *Geol. Soc. America Spec. Pap.,* 370, 209–230.

Da Silva, A.-C., Potma, K., Weissenberger, J. A. W., Whalen, M. T., Humblet, M., Mabille, C., Boulvain, F., 2009. Magnetic susceptibility evolution and sedimentary environments on carbonate platform sediments and atolls, comparison of the Frasnian from Belgium and Alberta, Canada. *Sed. Geol.*; 2014, 3-18. doi:10.1016/j.sedgeo.2008.01.010

Da Silva, A.-C., Dekkers, M. J., Mabille, C., Boulvain, F., 2012. Magnetic susceptibility and its relationship with paleoenvironments, diagenesis and remagnetization: examples from the Devonian carbonates of Belgium. *Stud. Geophys. Geod.*; 56, 677-704. doi:10.1007/s11200-011-9005-9

Da Silva, A.-C., Dekkers, M. J., De Vleeschouwer, D., Hladil, J., Chadimova, L., Slavík, L., Hilgen, F. J., 2018. Millenial-scale climate changes manifest Milankovitch combination tones and Hallstatt solar cycles in the Devonian greenhouse world. *Geology*; 47, 19-22. https://doi.org/10.1130/G45511.1

Da Silva, A.-C., Sinnesael, M., Claeys, P., Davies, J. H. F. L., de Winter, N. J., Percival, L. M. E., Schaltegger, U., De Vleeschouwer, D., 2020. Anchoring the Late Devonian mass extinction in absolute time by integrating climatic controls and radio-isotopic dating. *Sci. Rep.*; 10, 12940. https://doi.org/10.1038/s41598-020-69097-6.

https://doi.org/10.5194/egusphere-2026-2034
Preprint. Discussion started: 27 May 2026

De Vleeschouwer, D., Da Silva, A.-C., Boulvain, F., Crucifix, M. & Claeys, P., 2012. Precessional and half-precessional climate forcing of Mid-Devonian monsoon-like dynamics. *Clim. Past.*; 8, 337–351.

De Vleeschouwer, D., Crucifix, M., Bounceur, N. & Claeys, P., 2014. The impact of astronomical forcing in the Late Devonian greenhouse climate. *Glob. Planet. Change*; 120, 65–80.

De Vleeschouwer, D., Da Silva, A.-C., Sinnesael, M., Chen, D., Day, J. E., Whalen, M. T., Guo, Z., Claeys, P., 2017. Timing and pacing of the Late Devonian mass extinction event regulated by eccentricity and obliquity. *Nat. Comm.*; 8, 2268. doi:10.1038/s41467-017-02407-1.

De Vleeschouwer, D., Percival, L. M. E., Wichern, N. M. A., Batenburg, S. J., 2024. Pre-Cenozoic cyclostratigraphy and palaeoclimate responses to astronomical forcing. *Nat. Rev. Earth Environ.*; 5, 56-75. https://doi.org/10.1038/s43017-023-00505-x.

de Witt, Jr., W., and Colton, G. W., 1978. Stratigraphy and conodonts of the Genesee Formation (Devonian) in western and central New York. U. S. Geological Survey Professional Paper, 1032-A, 22 pp., 7 pl.

Ellwood, B. B., Crick, R. E., El Hassani, A., Benoist, S. L., Young, R. H., 2000. Magnetosusceptibility event and cyclostratigraphy method applied to marine rocks: Detrital input versus carbonate productivity. *Geology*; 28, 12, 1135-1138. https://doi.org/10.1130/0091-7613(2000)028<1135:MEACMA>2.3.CO;2

Gérard, J., Pohl, A., Sablon, L., Huygh, J. J. C., Da Silva, A.-C., Crucifix, M., 2026. Spatially contrasted response of Devonian anoxia to astronomical forcing. *EGUsphere*, 2025-4238 (preprint). https://doi.org/10.5194/egusphere-2025-4238

Gérard, J., Sablon, L., Huygh, J. J. C., Da Silva, A.-C., Pohl, A., Vérard, C., Crucifix, M., 2025. Exploring the mechanisms of Devonian oceanic anoxia: impact of ocean dynamics, palaeogeography, and orbital forcing. *Clim. Past*; 21, 239-260. https://doi.org/10.5194/cp-21-239-2025.

Hagelberg, T., Pisias, N., Elgar, S., 1991. Linear and nonlinear couplings between orbital forcing and the marine $\delta^{18}O$ record during the late Neogene. *Paleoceanogr.*; 6, 6, 729-746.

Hasselmann, K., Munk, W., MacDonald, G., 1963. Bispectra of Ocean Waves, Chapter 8 In: Proceedings of the Symposium on Time Series Analysis held at Brown University, June 11-14, 1962, Rosenblatt, M. (ed.). *John Wiley & Sons, Inc.*; 125-139

Hays, J. D., Imbrie, J. & Shackleton, N. J., 1976. Variations in the Earth's orbit: pacemaker of the ice ages. *Science* 194, 1121–1132.

Hinich, M.J., 1982. Testing for Gaussianity and linearity of a stationary time series. *J. Time Ser. Anal.*; 3, 3, 169-176.

Huybers, P. J. and Wunsch, C., 2004. A depth-derived Pleistocene age-model: Uncertainty estimates, sedimentation variability, and nonlinear climate change. *Paleoceanogr.*; 19, PA1028, 1-24. doi:10.1029/2002PA000857

Huygh, J. J. C., Algeo, T. J., Sageman, B. B., Arts, M. C. M., Ver Straeten, C. A., Over, D. J., Gérard, J., Sablon, L., Crucifix, M., Da Silva, A.-C., 2026. *Glob. Plan. Change*; 257:105216. https://doi.org/10.1016/j.gloplacha.2025.105216

Imbrie, J. and Imbrie, J. Z., 1979. Modeling the climatic response to orbital variations. *Science*; 207, 29, 943-953.

Jerolmack, D. J. and Paola, C., 2010. Shredding of environmental signals by sediment transport. *Geophys. Res. Lett.*; 37, 19, L19401. doi:10.1029/2010gl044638

Kirchgasser, W. T., 1994. Early morphotypes of Ancyrodella rotundiloba at the Middle/Upper Devonian boundary. In: Studies in Stratigraphy and Paleontology in honor of D. W. Fisher, E. Landing (ed.), New York State Museum Bulletin, 481, 117-134.

Klapper, G. (1989). The Montagne Noire Frasnian (Upper Devonian) conodont succession. In: McMillan, J.N., Embry, A.F., Glass, D. J. (eds.), Devonian of the World, *CSPG Memoir*, 14, 3, 449-468.

Lachaux, J.-P., Rodriguez, E., Martinerie, J., Varela, F.J., 1999. Measuring phase synchrony in brain signals. *Hum. Brain Mapping*; 8, 194-208.

Laurin, J., Meyers, S. R., Uličný, D., Jarvis, I., Sageman, B. B., 2015. Axial obliquity control on the greenhouse carbon budget through middle- to high-latitude reservoirs. *Paleoceanogr.;* 30, 2, 133-149. https://doi.org/10.1002/2014PA002736

Laskar, J., 2020. Astrochronology. In: Gradstein, F. M., Ogg, J. G., Schmitz, M. D. And Ogg, G. (eds.), *The Geologic Time Scale 2020*, chapter 4, 139-158.

Laskar, J., Robutel, P., Joutel, F., Gastineau, M., Correia, A. C. M., Levrard, B., 2004. A long-term numerical solution for the insolation quantities of the Earth. *Astron. Astrophys.*; 428, 1, 261-285. https://doi.org/10.1051/0004-6361:20041335.

https://doi.org/10.5194/egusphere-2026-2034
Preprint. Discussion started: 27 May 2026

Lourens, L. J., Sluijs, A., Kroon, D., Zachos, J. C., Thomas, E., Röhl, U., Bowles, J., Raffi, I., 2005. Astronomical pacing of late Paleocene to early Eocene global warming events. *Nature*; 435, 1083-1087. doi:10.1038/nature03814

Meyers, S. R., 2012. Seeing red in cyclic stratigraphy: Spectral noise estimation for astrochronology. *Paleoc.*; 27, PA3228. doi:10.1029/2012PA002307

Meyers, S. R., 2014. Astrochron: An R Package for Astrochronology. https://cran.r-project.org/package=astrochron

Meyers, S. R., 2015. The evaluation of eccentricity-related amplitude modulation and bundling in paleoclimate data: An inverse approach for astrochronologic testing and time scale optimization. *Paleoceanogr.*; 30, 12, 1625-1640. https://doi.org/10.1002/2015PA002850.

Meyers, S. R. and Hinnov, L. A., 2010. Northern hemisphere glaciation and the evolution of Plio-Pleistocene climate noise. Paleoceanogr.; 25, PA3207, 1-11. https://doi.org/10.1029/2009PA001834

Meyers, S. R., Sageman, B. B., Hinnov, L. A., 2001. Integrated quantitative stratigraphy of the Cenomanian-Turonian Bridge Creek limestone member using evolutive harmonic analysis and stratigraphic modeling. J. Sed. Res.; 71, 4, 628-644. doi:10.1306/012401710628

Milankovitch, M., 1974. Kanon der Erdbestrahlung und seine Anwendung auf das Eiszeitenproblem, *Royal Serbian Academy Special Publication*,133, 1-633

Mudelsee, M., 2010. Climate time series analysis: Classical statistical and bootstrap methods. *Springer*. ISBN 978-90-481-9481-0. Doi:10.1007/978-90-481-9482-7

Mulder, T., Syvitski, J. P. M., Migeon, S., Faugères, J.-C., Savoye, B., 2003. Marine hyperpycnal flows: initionation, behavior and related deposits. A Review. Mar. Pet. Geol., 20, 861-882. doi:10.1016/j.marpetgeo.2003.01.003

Paillard, D., 1998. The timing of Pleistocene glaciations from a simple multiple-state climate model. *Nature*; 391, 378-381.

Raup, D. M. and Sepkoski, J. J., Jr., 1982. Mass extinctions in the marine fossil record. *Science;* 215, 4539, 1501-1503. doi:10.1126/science.215.4539.1501.

Rial, J. A., Pielke, R. A. Sr., Beniston, M., Claussen, M., Canadell, J., Cox, P., Held, H., De Noblet-Ducoudré, N., Prinn, R., Reynolds, J. F., Salas, J. D., 2004. Nonlinearities, feedbacks and critical thresholds within the Earth's climate system. *Clim. Change.*; 65, 11-38.

Rickard, L. V. 1975. Correlation of the Silurian and Devonian Rocks in New York State. New York State Museum and Science Service, Map and Chart Series, 24, 16 pp. and 4 pl.

Rosenblum, M. G., Pikovsky, A. S., Kurths, J., 1996. Phase synchronization of chaotic oscillators. *Phys. Rev. Lett.*; 76, 11, 1804-1807.

Saltzman, B. (2002). Dynamical Paleoclimatology: Generalized Theory of Global Climate Change. Academic Press, San Diego, 354 pp, ISBN 0-12-617331-1.

Schneider, T., Bischoff, T., Haug, G.H., 2014. Migrations and dynamics of the intertropical convergence zone. *Nature*; 513, 45-53. doi:10.1038/nature13636

Scotese, C. R., 2021. An atlas of Phanerozoic paleogeographic maps: The seas come in and the seas go out. *Annu. Rev. Earth Planet. Sci.*; 49, 669-718. https://doi.org/10.1146/annurev-earth-081320-064052

Stein, W. E., Berry, C. M., Morris, J. L., VanAller Hernick, L., Mannolini, F., Ver Straeten, C., Landing, E., Marshall, J. E. A., Wellman, C. H., Beerling, D. J., Leake, J. R., 2020. Mid-Devonian *Archeopteris* roots signal revolutionary change in earliest fossil forests. *Curr. Biol.*; 30, 1-11. doi:10.1016/j.cub.2019.11.067

Sullivan, N. B., Meyers, S. R., Levy, R. H., McKay, R. M., Golledge, N. R., Cortese, G., 2023. Millennial-scale variability of the Antarctic ice sheet during the early Miocene. *Earth Atmos. Planet. Sci.*; 120, 39, 1-8, e2304152120. https://doi.org/10.1073/pnas.2304152120

Thomson, D. J., 1982. Spectrum estimation and harmonic analysis. *Proc. IEEE*; 70, 9, 1055-1096.

Tucker, G. E., and Slingerland, R., 1997. Drainage basin responses to climate change. *Water Resour. Res.*; 33, 8, 2031-2047. doi:10.1029/97wr00409

Tuenter, E., Weber, S. L., Hilgen, F. J., Lourens, L. J., 2003. The response of the African summer monsoon to remote and local forcing due to precession and obliquity. *Glob. Plan. Change;* 36, 219-235. doi:10.1016/S0921-8181(02)00196-0

Ver Straeten, C. A., 2010, Lessons from the foreland basin: Northern Appalachian basin perspectives on the Acadian orogeny. In: Tollo, R. P., Bartholomew, M. J., Hibbard, J. P., and Karabinos, P. M., (eds.), From

https://doi.org/10.5194/egusphere-2026-2034
Preprint. Discussion started: 27 May 2026

Rodinia to Pangea: The Lithotectonic Record of the Appalachian Region: Geological Society of America Memoir 206, 251–282, doi: 10.1130/2010.1206(12).

Ver Straeten, C. A., Over, D. J., & Woodrow, D. L. (eds.). 2023. Devonian of New York, Volume 2: Lower to Upper Givetian (Middle Devonian) Stage. *Paleontol. Res. Inst., Bull. Am. Paleontol*.

Ver Straeten, C. A., 2023. An introduction to the Devonian Period, and the Devonian in New York State and North America. In: Ver Straeten, C. A., Over, D. J. and Woodrow, D. (eds.), Devonian of New York, Volume 1: Introduction and Přídolí to lower Givetian (Upper Silurian to Middle Devonian) stages. *Bull. Am. Paleontol.;* 403-404. doi:10.32857/bap.2023.403.03

von Dobeneck, T., and Schmieder, F., 1999. Using rock magnetic proxy records for orbital tuning and extended time series analysis into the super- and sub-Milankovitch bands. In: Use of proxies in paleoceanography: Examples from the South Atlantic, Fischer, G., Wefer, G., (eds.), *Springer-Verlag Berlin Heidelberg*, 601-603.

Waltham, D., 2015. Milankovitch period uncertainties and their impact on cyclostratigraphy. *J. Sed. Res.*; 85, 990-998. https://doi.org/10.2110/jsr.2015.66

Wichern, N. M. A., Bialik, O. M., Nohl, T., Percival, L. M. E., Becker, T. R., Kaskes, P., Claeys, P., De Vleeschouwer, D., 2024. Astronomically paced climate and carbon cycle feedbacks in the lead-up to the Late Devonian Kellwasser Crisis. *Clim. Past;* 20, 415-448. https://doi.org/10.5194/cp-20-415-2024

Wilson, R. D. and Schieber, J., 2014. Muddy prodeltaic hyperpycnites in the lower Genesee Group of Central New York, USA: Implications for mud transport in epicontinental seas. *J. Sediment. Res.*, 84, 866-874. http://dx.doi.org/10.2110/jsr.2014.70

Wilson, R. D. and Schieber, J., 2015. Sedimentary facies and depositional environment of the Middle Devonian Geneseo Formation of New York, USA. *J. Sediment. Res.*, 85, 1393-1415. http://dx.doi.org/10.2110/jsr.2015.88

Wilson, R. D. and Schieber, J., 2017. Association between wave- and current-aided hyperpycnites and flooding surfaces in shelfal mudstones: An integrated sedimentological, sequence stratigraphic, and geochemical approach. *J. Sediment. Res.*, 87, 1143-115. http://dx.doi.org/10.2110/jsr.2017.62

Witzke, B. J., Bunker, B. J., and Rogers, F. S., 1988. Eifelian through lower Frasnian stratigraphy and deposition in the Iowa area, Midcontinent, U.S.A., In: McMillan, N. J., Embry, A. F., and Glass, D. J., (eds.), Devonian of the World; proceedings of the 2nd international symposium on the Devonian System; Volume I, Regional synthesis: *CSPG Memoir*, 14, 221-250.

Witzke, B. J., Bunker, B. J., 1996. Relative sea-level changes during the Middle Ordovician through Mississippian deposition in the Iowa area, North American Craton. In: Paleozoic Sequence Stratigraphy, Witzke, B. J., Ludvigson, G. A., Day, J. (eds.). *GSA Spec. Pap.* ISBN 9780813723068. https://doi.org/10.1130/0-8137-2306-X.307

Witzke, B. J., Bunker, B. J., 1997. Sedimentation and stratigraphic architecture of a Middle Devonian (late Givetian) transgressive-regressive carbonate-evaporite cycle, Coralville Formation, Iowa area. In: Paleozoic sequence stratigraphy, biostratigraphy, and biogeography, Klapper, G., Murphy, M. A., Talen, J. A. (eds.). *GSA Spec. Pap.* ISBN 9780813723211. https://doi.org/10.1130/SPE321

Wu, Z., Yin, Q., Berger, A., Guo, Z., 2025. Forcing mechanisms of the half-precession cycle in the wester equatorial Pacific temperature. *Nat. Commun.*; 16, 1841. https://doi.org/10.1038/s41467-025-57076-2

Zambito, J., Baird, G., Brett, C., and Bartholomew, A., 2009. Depositional sequences and paleontology of the Middle – Upper Devonian transition (Genesee Group) at Ithaca, New York: a revised lithostratigraphy for the Northern Appalachian Basin, In: Studies in Devonian Stratigraphy, Over, D. J. (ed.). *Paleontogr. Am.*; 63, 49-69.

Zambito, J.J. IV, Brett, C. E., Baird, G. C., 2012. The late Middle Devonian (Givetian) global Taghanic biocrisis in its type area (northern Appalachian Basin): Geologically rapid faunal transitions driven by global and local environmental changes. In: *Earth and Life*, International Year of Planet Earth, Talent, J. A. (ed.), 677-703. doi:10.1007/978-90-481-3428-1_22

Zambito, J. J. IV, Day, J. E., and Narkiewicz, K., 2015. New insights in the trilobite and conodont biostratigraphy of the Middle-Upper Devonian Genesee Group in eastern New York State. P. 154, In: IGCP 596–SDS Symposium: Climate Change and Biodiversity Patterns in the Mid-Palaeozoic, Mottequin, B., Denayer, J., Königshof, P., Prestianni, C., and Olive, S. (eds.), *STRATA*, série 1: Communications, 16.

Zambito, J.J. IV, Joachimski, M. M., Brett, C. E., Baird, G. C., Aboussalam, Z. S., 2016. A carbonate isotope record for the late Givetian (Middle Devonian) global Taghanic biocrisis in the type region (northern Appalachian Basin). In: *Devonian Climate, Sea Level and Evolutionary Events*, Becker, R. T., Königshof, P., and Brett, C. E. (eds.), Geological Society, London, Special Publications, 423, 223-233. http://doi.org/10.1144/SP423.7

https://doi.org/10.5194/egusphere-2026-2034
Preprint. Discussion started: 27 May 2026

1045 Zeebe, R. E. and Lantink, M. L., 2024. A secular solar system resonance that disrupts the dominant cycle in
1046 Earth's orbital eccentricity (g_2-g_5): Implications for astrochronology. *Astron. J.*; 167:204.
1047 https://doi.org/10.3847/1538-3881/ad32cf.

1048 Zeeden, C., Meyers, S., Hilgen, F., Lourens, L., Laskar, J., 2019. Time scale evaluation and the quantification of
1049 obliquity forcing. *Quat. Sci. Rev.*; 209, 100-113. https://doi.org/10.1016/j.quascirev.2019.01.018.

1050 Zhang, T., Li, Y., Fan, T., Da Silva, A.-C., Kuang, M., Liu, W., Ma, C., Gao, Q., Shi, J., Gao, Z., & Li, M., 2022.
1051 Orbital forcing of tropical climate dynamics in the Early Cambrian. *Glob. Planet. Change*; 219, 103985.
1052 https://doi.org/10.1016/j.gloplacha.2022.103985